**Supporting Information**

**Ru Atomic Clusters-installed Co-Co$_2$B Nanocatalyst Remarkably Combats Product Inhibition While Sustaining High Turnover Frequency of Hydrogen Production**†

Rajani Kumar Borah,[ac] Priti Singh,[b] Mudit Dixit[bc] and Amit A. Vernekar*[ac]

[a]Inorganic and Physical Chemistry Laboratory

CSIR-Central Leather Research Institute (CLRI), Adyar, Chennai-600020, India

E-mail: amitvernekar@clri.res.in

[b]Advanced Materials Laboratory

CSIR-Central Leather Research Institute (CLRI), Adyar, Chennai-600020, India.

[c]Academy of Scientific and Innovative Research (AcSIR), Ghaziabad-201002, India.

**Table of contents**

# 1. Materials and methods

## 1.1 Chemicals and materials

Methanol (MeOH, HPLC gradient grade, Thermo Fisher Scientific India Pvt. Ltd.), Cobalt (II) chloride hexahydrate ($CoCl_2.6H_2O$, SD Fine-Chem Ltd.), Ruthenium trichloride ($RuCl_3.3H_2O$, Molychem), Phenolphthalein 1% indicator solution (Merck), Methanol-OD (Sigma), and Milli-Q water were used as received. Ammonia borane (AB, $NH_3BH_3$) was synthesized using Ammonium sulphate extrapure AR grade (Sisco Research Laboratories Pvt. Ltd.) and Sodium borohydride extrapure (Sisco Research Laboratories Pvt. Ltd.) in Tetrahydrofuran (HPLC grade, Rankem) by following the procedure described by Ramachandran and Gagare.[1] Graphitic carbon nitride (g-$C_3N_4$) was synthesized *via* pyrolysis of melamine (HiMedia Laboratories Pvt. Ltd.) at 520°C in a muffle furnace for 2 h as described by Wang et al.[2]

## 1.2. Synthetic methods

### Synthesis of Co-Co₂B catalysts

In a Schlenk tube, 2 mL of MeOH was combined with 0.1 mmol of $CoCl_2.6H_2O$. While sonicating at 60°C, an excess amount of AB was introduced to this solution, resulting in the formation of a black precipitate identified as Co-$Co_2B$, accompanied by the evolution of gas bubbles. The catalyst was isolated using a magnet and washed twice with MeOH. Subsequently, the dehydrogenation activity of the catalyst was investigated.

### Synthesis of (1, 2.5, 5, 10, 25, 50) % RuACs/Co-Co₂B catalysts

In the Schlenk tube containing 2 mL MeOH, varying amounts of $CoCl_2.6H_2O$ (0.099, 0.0975, 0.095, 0.09, 0.075, 0.05 mmol) and $RuCl_3.3H_2O$ (0.001, 0.0025, 0.005, 0.01, 0.025, 0.05 mmol) were added to prepare 1, 2.5, 5, 10, 25, 50 % RuACs/Co-$Co_2B$ catalysts, respectively. To this solution, an excess of AB was added under sonication leading to the formation of a black precipitate with the evolution of hydrogen gas. The resulting 1, 2.5, 5, 10, 25, 50 % RuACs/Co-$Co_2B$ catalysts were isolated using a magnet and subjected to two washes with MeOH. Subsequently, the dehydrogenation activity of each catalyst was investigated.

### Synthesis of Ru nanoparticles (NPs)

In a Schlenk tube containing 2 mL MeOH, 0.1 mmol of $RuCl_3.3H_2O$ was added. An excess amount of AB was introduced to the solution under sonication, leading to the formation of a black precipitate consisting of Ru NPs, accompanied by the evolution of hydrogen gas. The resulting catalyst was isolated by centrifugation and washed twice with MeOH. Subsequently, the dehydrogenation activity of the catalyst was investigated.

## 1.3. Characterization

Scanning electron microscopy (SEM) imaging was performed on Tescan Clara scanning electron microscope. Powder XRD analysis was performed on Rigaku mini flex-II desktop (Cu Kα 1.5406 Å radiation). X-ray photoelectron spectroscopy (XPS) was recorded on a MULTILAB 2000 THERMO SCIENTIFIC, UK. Transmission electron microscopy (TEM)

images and selected area electron diffraction (SAED) patterns were recorded on the JEOL (JEM 2100 Plus electron microscope) and Talos F200X G2 transmission electron microscopes. NMR experiments were performed using Bruker Ascend 400 MHz spectrometer. Metal content was studied using Agilent 7700 series Inductively Coupled Plasma Mass Spectrometry (ICP-MS).

### 1.4. $H_2$ generation experiments

### 1.4.1. Dehydrogenation of AB

1 mL of 0.5 M AB solution was injected, while stirring, into the Schlenk tube (containing freshly prepared catalysts synthesized using the procedure given in 1.2 section) placed in a water bath maintained at room temperature. The volume of the $H_2$ gas generated per unit time was measured by recording the volume of water displaced from the burette. The final volume of the $H_2$ gas generated was found by equalizing the level of the water in the reservoir with the level of the water in the gas burette. The experiments were conducted in triplicate sets and the graphs were plotted using the Origin software.

### 1.4.2. Activity of Co-Co$_2$B, (1, 2.5, 5, 10, 25, 50) % RuACs/Co-Co$_2$B, and Ru NPs towards dehydrogenation of AB

The catalytic activities of the prepared Co-Co$_2$B, (1, 2.5, 5, 10, 25, 50) % RuACs/Co-Co$_2$B and 100 % Ru were studied for dehydrogenation of AB according to the procedure (1.4.1). The experiments were conducted in triplicate and the rate and TOF was calculated for each catalyst.

### 1.4.3. Catalyst (10% RuACs/Co-Co$_2$B) amount variation for dehydrogenation of AB

0.5, 1, 1.5, 2, 2.5 times 10% RuACs/Co-Co$_2$B catalysts were synthesized and tested for AB dehydrogenation activity by adding 1 mL of 0.5 M AB solution separately to the Schlenk tube. The gas generated was measured according to procedure (1.4.1). The experiments were conducted in triplicate and the rate for each reaction was calculated.

### 1.4.4. Dehydrogenation of AB at different temperature using 10% RuACs/Co-Co$_2$B and Co-Co$_2$B catalyst

Dehydrogenation of AB at 283, 293, 303, and 313 K by 10% RuACs/Co-Co$_2$B and Co-Co$_2$B catalyst was investigated separately according to procedure (1.4.1). The experiments were conducted in triplicate and the rate for each reaction was calculated.

### 1.4.5. Dehydrogenation activity with different AB concentrations using 10% RuACs/Co-Co$_2$B and Co-Co$_2$B catalysts

10% RuACs/Co-Co$_2$B catalyst was synthesized in the Schlenk tube and its catalytic activity was checked by adding 1 mL of 0.25, 0.375, 0.5, 0.625, 0.75, 0.875 and 1 M AB solution according to procedure (1.4.1). The experiments were conducted in triplicate and the rate for each reaction was calculated.

The dehydrogenation activity of Co-Co$_2$B catalyst with 1 mL of 0.25, 0.375, 0.5, 0.625, 0.75, 0.875 and 1 M AB solution was also investigated solution according to procedure (1.4.1). The experiments were conducted in triplicate and the rate for each reaction was calculated.

### 1.4.6. Reusability test of 10% RuACs/Co-Co$_2$B for dehydrogenation of AB

After the first cycle of AB dehydrogenation by 10% RuACs/Co-Co$_2$B catalyst, it was separated with the help of a magnet and the clear supernatant solution was discarded. The used catalyst was washed once with MeOH and it was reused for AB dehydrogenation according to the procedure (1.4.1). Similarly, the activity of the catalyst was checked for 10 consecutive catalytic cycles and the rate for each cycle was calculated.

### 1.4.7. Experiments for testing prevention of product inhibition

### 1.4.7.1. Preparation of ammonium tetramethoxyborate (NH$_4$B(OMe)$_4$, AMB) stock solution (2M)

To the Schlenk tube containing synthesized 10% RuACs/Co-Co$_2$B catalyst, 1 mL of 2M AB solution was injected. After complete methanolysis of AB, the supernatant was collected and centrifuged. This solution has 2 M AMB.

### 1.4.7.2. Studies of inhibition of AB dehydrogenation by using AMB

To the Schlenk tube containing synthesized 10% RuACs/Co-Co$_2$B catalyst, appropriate volumes of 2 M AMB stock solution was added to result in final 0.5, 1 and 1.5 M AMB. The reaction mixture was sonicated for ~1 min. To this mixture, an appropriate volume of MeOH containing 0.5 mmol of AB was added and the activity was tested following the aforementioned procedure (1.4.1).

The same experiment was also performed for the Co-Co$_2$B catalyst with (0.5, 1, 1.5) M of AMB.

### 1.4.8. Testing AB dehydrogenation by 90% Co-Co$_2$B catalyst (control catalyst 1)

The catalyst was synthesized by reducing 0.09 mmol of CoCl$_2$.6H$_2$O in the presence of AB at 60°C. The black precipitate of Co-Co$_2$B was formed with the evolution of gas bubbles. The catalyst was separated using a magnet and washed twice with MeOH. Then, the dehydrogenation activity of the catalyst was investigated following the aforementioned procedure (1.4.1).

Note: 90% Co-Co$_2$B corresponds to the catalyst prepared using the amount of CoCl$_2$.6H$_2$O required for making 10% RuAC/Co-Co$_2$B.

### 1.4.9. Testing AB dehydrogenation by 10% Ru NPs (control catalyst 2)

In the Schlenk tube containing 2 mL MeOH, 0.01 mmol of RuCl$_3$.3H$_2$O was added. Excess amount of AB was added to this solution while sonicating to form a black precipitate of Ru NPs with the evolution of gas bubbles. The formed catalyst was isolated by centrifugation and washed twice with MeOH. Then, the dehydrogenation activity of the catalyst was investigated following the aforementioned procedure (1.4.1).

Note: 10% Ru NPs corresponds to the catalyst prepared using the amount of RuCl$_3$.3H$_2$O required for making 10% RuACs/Co-Co$_2$B.

**1.4.10.   AB dehydrogenation by 90% Co-Co$_2$B and 10% Ru NPs catalyst together (control catalyst 3 and 4)**

90% Co-Co$_2$B and 10% Ru NPs catalyst were synthesized in two different Schlenk tube by following aforementioned procedure 1.4.8 and 1.4.9, respectively. Then, both the catalysts were placed in the same Schlenk tube (control catalyst 3) and their activity for dehydrogenation of AB was tested following the aforementioned procedure (1.4.1).

In another experiment, first 90% Co-Co$_2$B catalyst was synthesized in a Schlenk tube and then 0.01 mmol of RuCl$_3$.3H$_2$O was added to the tube followed by reduction with excess AB while sonicating. After washing the catalyst (control catalyst 4) with MeOH for two times, its AB dehydrogenation activity was tested following the aforementioned procedure (1.4.1).

**1.4.11. Dehydrogenation of AB by 10% Ru NPs supported on g-C$_3$N$_4$ (control catalyst 5)**

7 mg g-C$_3$N$_4$ was dispersed in 2 mL of MeOH in a Schlenk tube.  Then, 0.01 mmol of RuCl$_3$.3H$_2$O was added to it and followed by reduction with AB while sonicating. The formed black color catalyst (control catalyst 5) was collected by centrifugation and washed two times with MeOH. Then, the dehydrogenation activity of the catalyst was investigated following the aforementioned procedure (1.4.1).

**1.4.12. Hydrolysis of AB by 10% RuACs/Co-Co$_2$B catalyst**

The Schlenk tube containing 10% RuACs/Co-Co$_2$B catalyst was placed in a water bath maintained at room temperature. Then, 1 mL of 0.5 M aqueous AB solution was injected by a syringe while stirring. The volume of the H$_2$ gas generated per unit time was measured by recording the volume of water displaced from the burette. The final volume of the H$_2$ gas generated was found by equalizing the level of the water in the reservoir with the level of the water in the gas burette. The experiments were conducted in triplicate sets and the graphs were plotted using the Origin software.

**1.4.13. Phenolphthalein test for detection of ammonia**

In a Schlenk tube containing 10% RuACs/Co-Co$_2$B catalyst, 1 mL of 0.5 M AB MeOH solution was injected by a syringe while stirring. The evolved gas was passed through a tube containing phenolphthalein solution.

In another Schlenk tube containing 10% RuACs/Co-Co$_2$B catalyst, 1 mL of 0.5 M aqueous AB solution was injected by a syringe while stirring. The evolved gas was passed through a tube containing phenolphthalein solution.

**1.4.14. Determination of Ru content in 10% RuACs/Co-Co$_2$B catalyst by ICP-MS**

After the synthesis of the catalyst following above discussed procedure, it was dried in N$_2$ flow. 5 mg of the catalyst was dissolved in 5 mL of conc. HNO$_3$. From this solution, an appropriate amount was taken to make 8 ppm 50 mL stock solution. To get 0.72 ppm Co and 0.4 ppm Ru as per calculations, this solution was serially diluted and analyzed by ICP-MS.

## 1.5. Calculation of turnover frequency (TOF)

The turnover frequency (TOF) was calculated by the following formula.

$$TOF = \frac{(\text{moles of } H_2 \text{ generated})}{(\text{moles of catalyst}) (\text{time})}$$

## 1.6. Plotting of ideal zero-order plot

A few initial data points from the actual reaction graph were extrapolated to obtain a straight line plot using the Origin software. The initial data points were chosen because, under the initial conditions, the production of borate is minimal to have any inhibitory effect.

## 1.7. Calculation of % product inhibition

The successive $t_{1/2}$ values were calculated for ideal and experimental plots. The slow-down of the reaction in the experimental reaction was calculated by comparing its $t_{1/2}$ values with respect to the $t_{1/2}$ values of the ideal plot. Finally, % inhibition was calculated by the difference of total % increase in the $t_{1/2}$ values in experimetal and 100 % $t_{1/2}$ values of ideal.

## 2. Computational methods

To understand the catalytic activity of Ru-clusters (Ru-13-, and Ru-19-atom), $Co_2B$ surface, and Ru-$Co_2B$ composite for AB methanolysis, we performed density functional theory (DFT) calculations as implemented in the Vienna Ab Initio Simulation package (VASP).[3,4] The exchange-correlation energy was computed by utilizing projector augmented wave (PAW) potentials, and Perdew-Burke-Erenzerhof (PBE) exchange-correlation functional within the generalized gradient approximation.[5] The kinetic energy cut-off was set to 520 eV with a Monkhorst-Pack $k$-point mesh of 5×5×5. The lowest-energy structures of Ru clusters with variable size (0.37 nm radius (13 atoms), 0.4 nm radius (19 atoms)) were relaxed with a $k$-point mesh of 1×1×1. Based on the experimental observations, surface calculations were performed for the most abundant facet of Ru (002) (36 Ru atoms), 211 facet of $Co_2B$ (96 atoms) with vacuum space of 12 Á. A larger slab model (with 211 atoms) was considered for identifying the lowest energy structures of Ru-$Co_2B$ composite systems. For the Ru (002) surface, one bottom layer was constrained and while two bottom layers were fixed for the $Co_2B$ systems at optimized bulk relaxed positions. To investigate the interaction between adsorbate (AB and MeOH) and catalyst surface and to assess the thermodynamic feasibility of AB methanolysis, we computed the adsorption energy ($\Delta E_{ads}$) for different intermediates using the CP2K package[6] with Grimme's D3 exchange-correlation functional.[7] The DZVP basis with the Goedecker, Teter, and Hutter (GTH) pseudopotentials was used with a kinetic energy cut-off of 500 Ry. The adsorption energies were computed using the following equation:

$$\Delta E_{ads} = E_{complex} - (E_{cat} + E_{adsorbate})$$

Where, $E_{complex}$ shows the free energy for adsorbed complex, $E_{cat}$ represents the free energy of catalyst, and $E_{adsorbate}$ shows the free energy for adsorbate species. The AB and MeOH adsorption takes place in the following steps,

$$NH_3BH_3 + MeOH + * \rightarrow *BH_3NH_3 + *MeOH \qquad (1)$$

$$*NH_3BH_3 + *MeOH \rightarrow *BH_2(OMe)NH_3 + *H_2 \uparrow \qquad (2)$$

$$*BH_2(OMe)NH_3 + *MeOH \rightarrow *BH(OMe)_2NH_3 + *H_2 \uparrow \qquad (3)$$

$$*BH_2(OMe)_2NH_3 + *MeOH \rightarrow *B(OMe)_3NH_3 + *H_2 \uparrow \qquad (4)$$

$$*B(OMe)_3NH_3 + *MeOH \rightarrow *B(OMe)_4NH_4 \qquad (5)$$
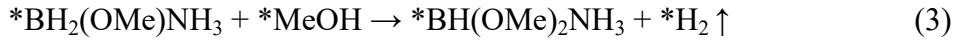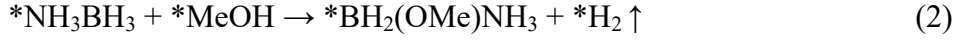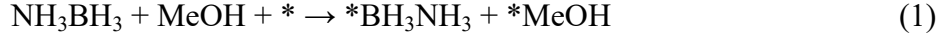
Where, * represents the adsorbed state, $Ru_{19}$-cluster, clean $Co_2B$ (211) facet, Ru (002) facet, and $Ru$-$Co_2B$. Further electronic structure calculations for all adsorbed intermediates were carried out using the VASP with a *k*-point mesh of 1×1×1. To understand the nature and strength of bonds between adsorbate and catalyst, we performed crystal orbital Hamilton population (COHP) analysis.[8,9]

## 3. Supplementary figures and tables
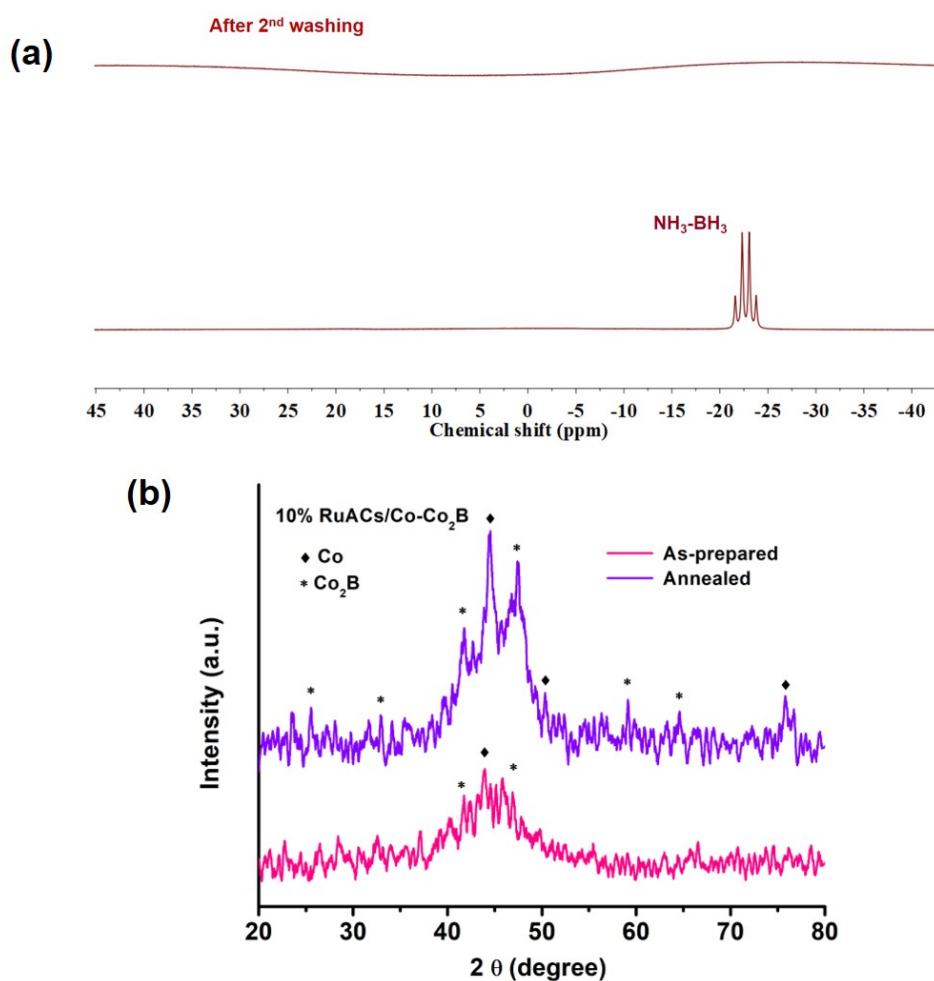


**Figure S1:** (a) $^{11}B$ NMR spectra of AB and the spectra recorded after 2nd washing of the synthesized 10% RuACs/Co-Co$_2$B catalyst, (b) Powder X-ray diffraction (XRD) patterns of 10% RuACs/Co-Co$_2$B.
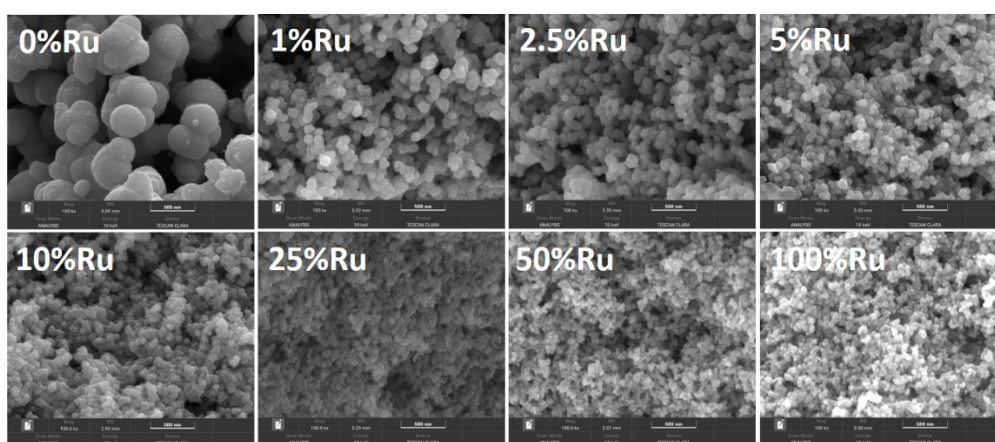


**Figure S2:** SEM images of Co-Co$_2$B catalyst with varied amount of Ru percentage, (scale bar 500 nm).

| Element | Atomic % |
| --- | --- |
| B K | 28.10 |
| Co L | 58.07 |
| Ru L | 13.83 |
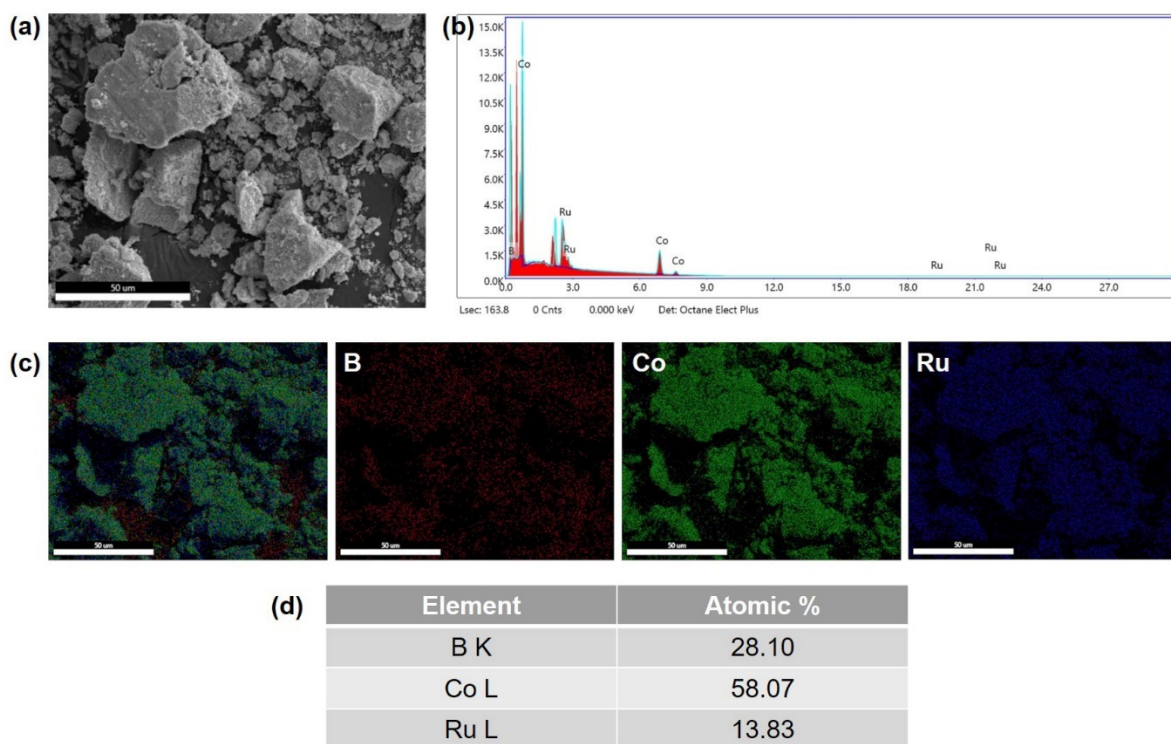
**Figure S3:** (a) SEM images of 10% RuACs/Co-Co$_2$B catalyst (scale bar 50 nm) and (b) its EDX spectrum (c) EDX mapping of 10% RuACs/Co-Co$_2$B showing the presence of B (red), Co (green), and Ru (blue), (d) Atomic % of elements present in the 10% RuACs/Co-Co$_2$B as obtained from EDX analysis.
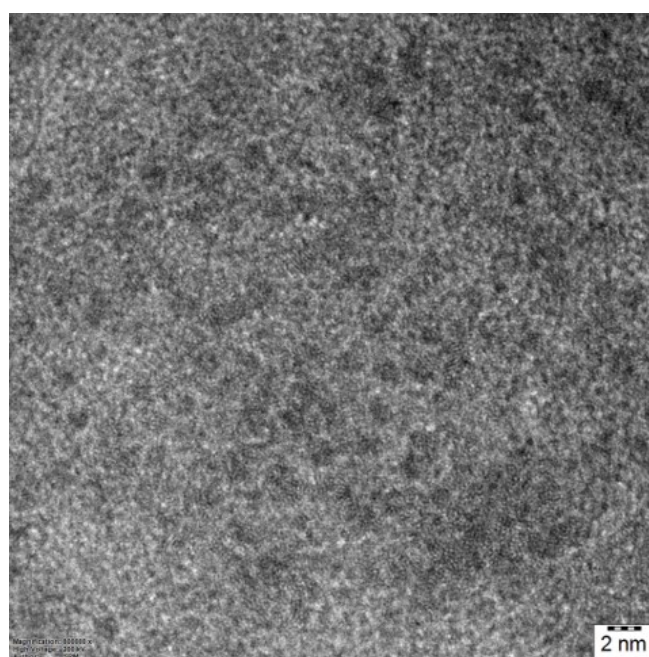


**Figure S4:** (a) HRTEM images of 10% RuACs/Co-Co$_2$B catalyst.
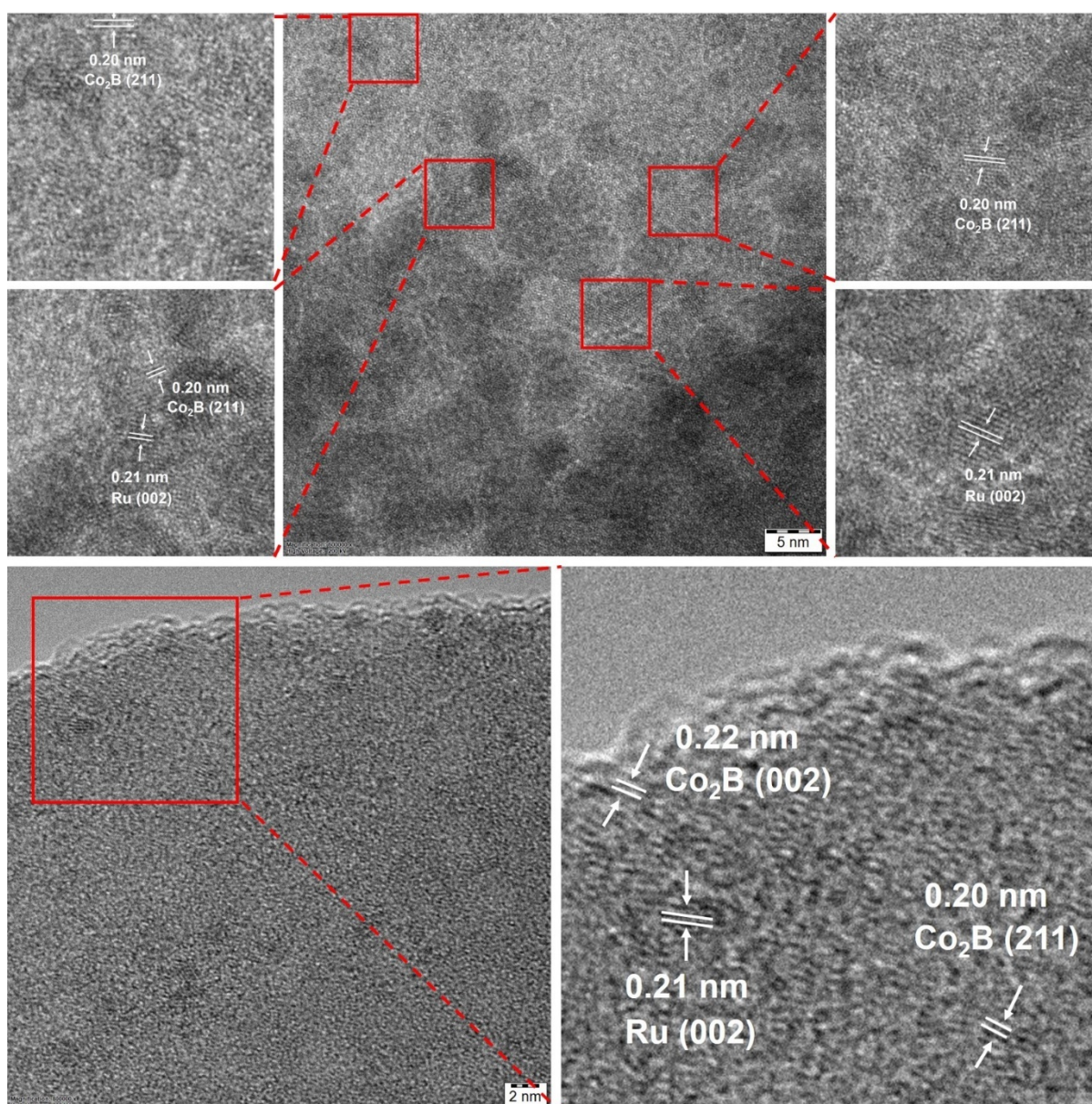
**Figure S5:** HRTEM images of as-synthesized 10% RuACs/Co-Co$_2$B showing the Ru clusters as dark spots and the lighter background portion as Co$_2$B. The short-range crystallinity of Co$_2$B is confirmed by magnifying the red box marked area, highlighting the lattice planes with d = 0.20 nm and 0.22 nm, corresponding to (211) and (002) planes. The lattice planes corresponding to Ru are also marked.
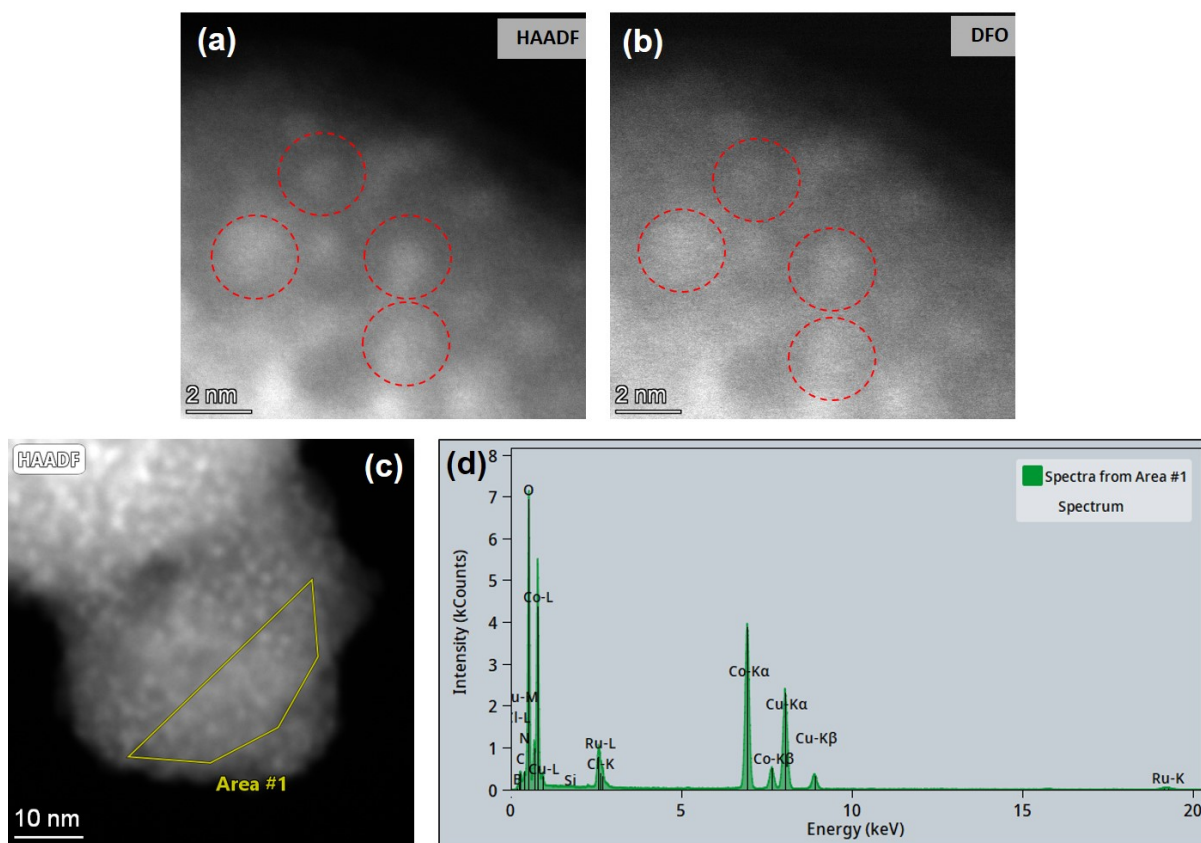
**Figure S6:** (b) HAADF, (c) DF images of 10% RuACs/Co-Co$_2$B catalyst, (d) HAADF STEM image of 10% RuACs/Co-Co$_2$B catalyst, and e) EDX spectra of the marked area in the image (d).
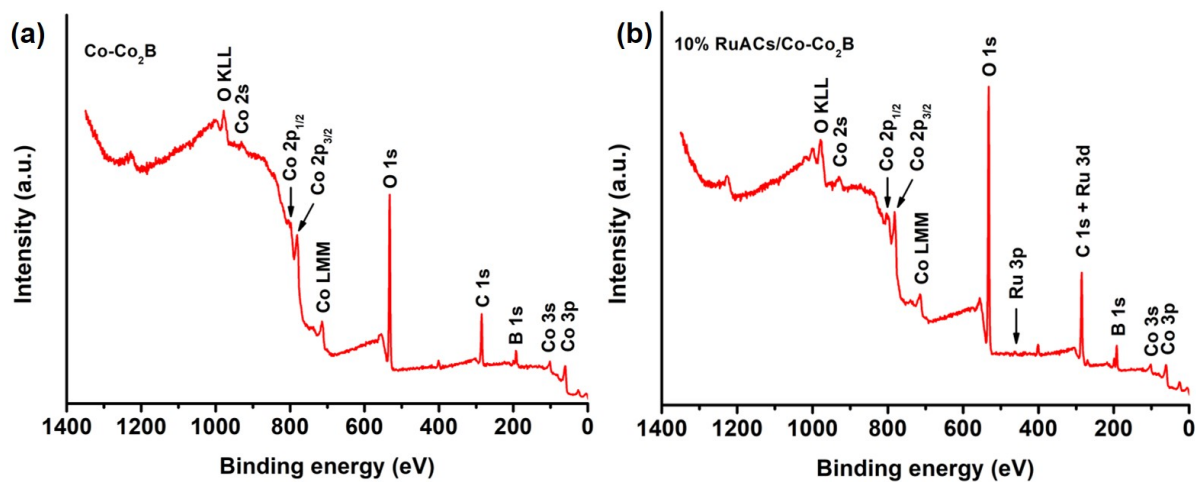


**Figure S7:** XPS survey spectra of (a) Co-Co$_2$B, (b) 10% RuACs/Co-Co$_2$B.
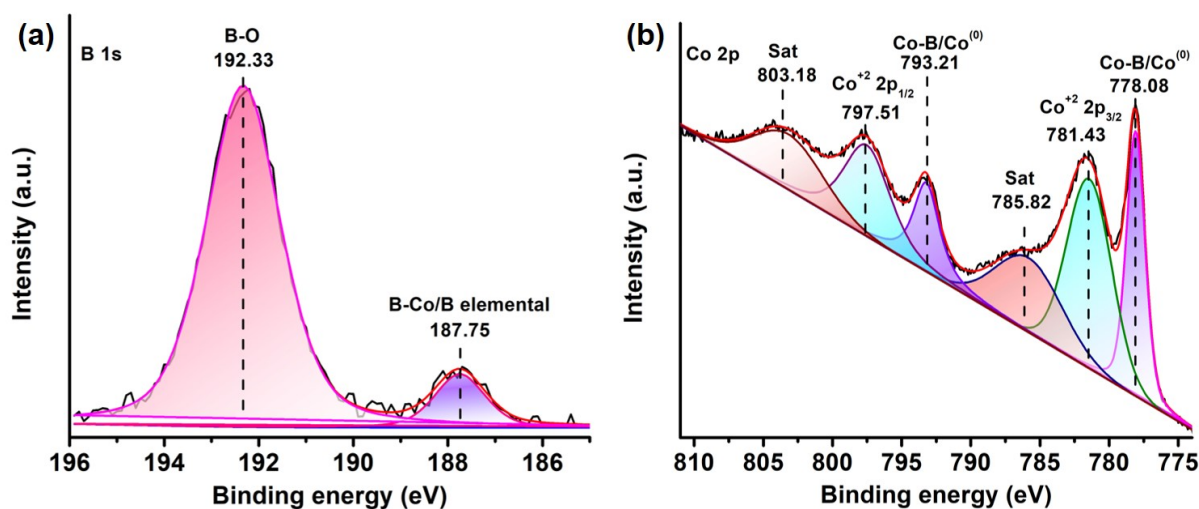
**Figure S8:** XPS Spectra of (a) B 1s, (b) Co 2p of Co-Co$_2$B catalyst.
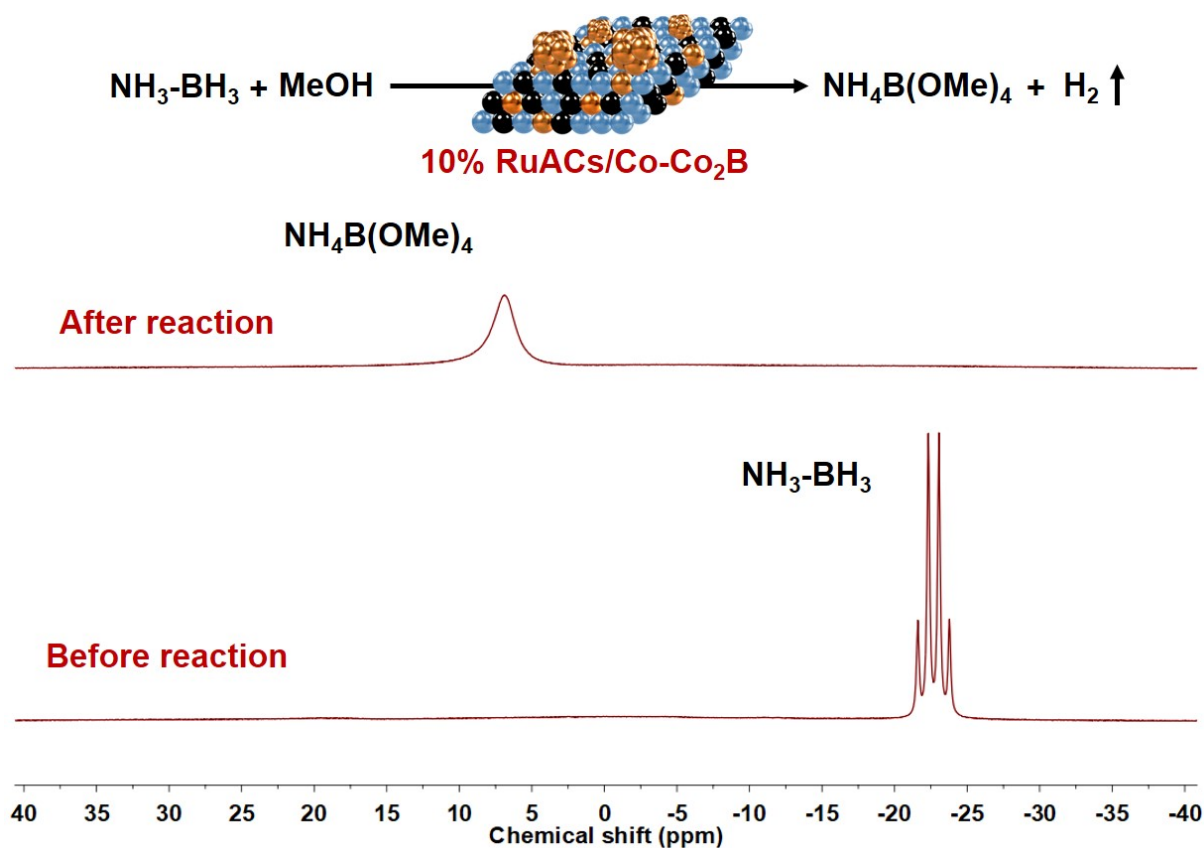


**Figure S9:** ^{11}B NMR spectra recorded before and after the AB dehydrogenation reaction by 10% RuACs/Co-Co$_2$B. The peak appearing at δ 6.89 ppm corresponds to NH$_4$B(OMe)$_4$ (AMB) in agreement with the previous report.[1]
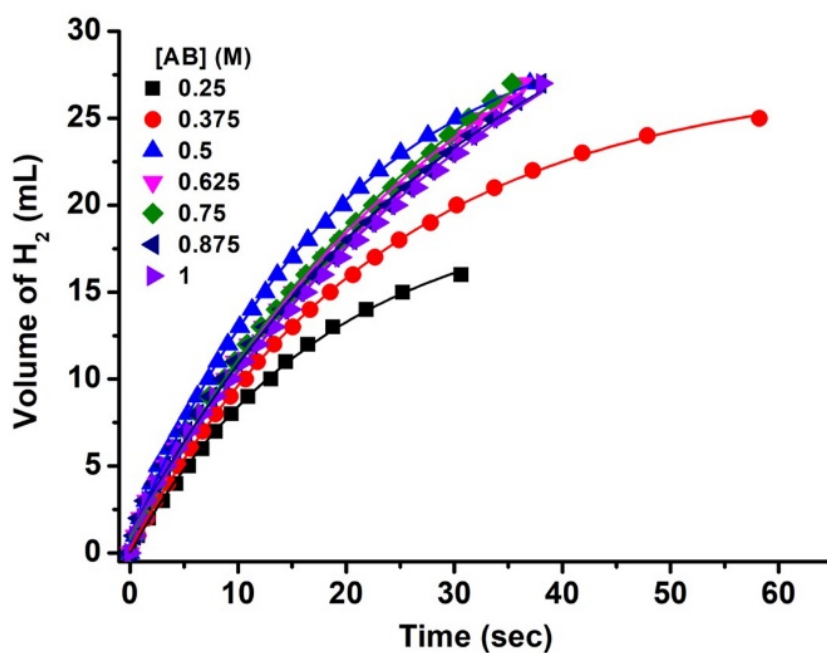
**Figure S10:** Effect of AB concentration variation on the dehydrogenation of AB by Co-Co$_2$B catalyst.
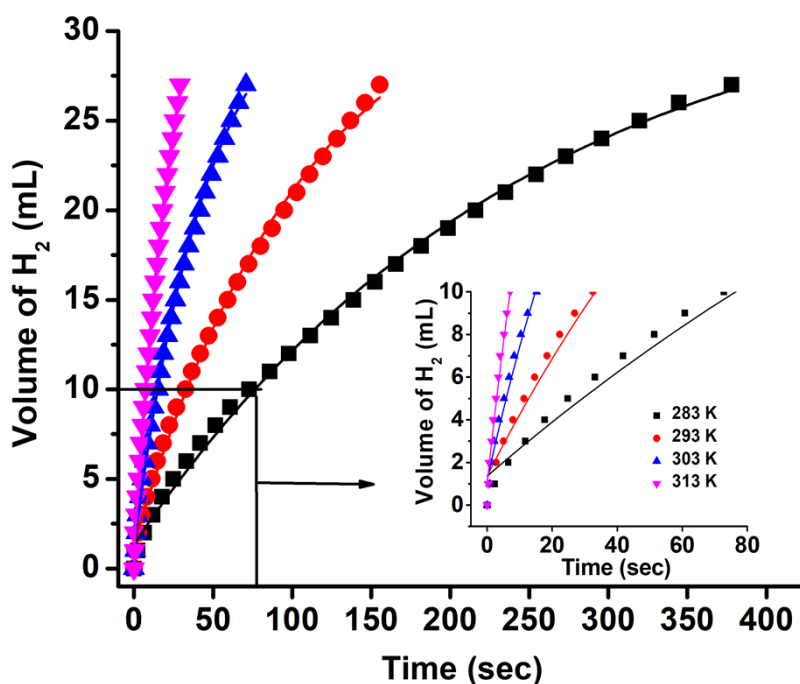


**Figure S11:** Effect of reaction temperature variation for hydrogen production from AB by Co-Co$_2$B catalyst.
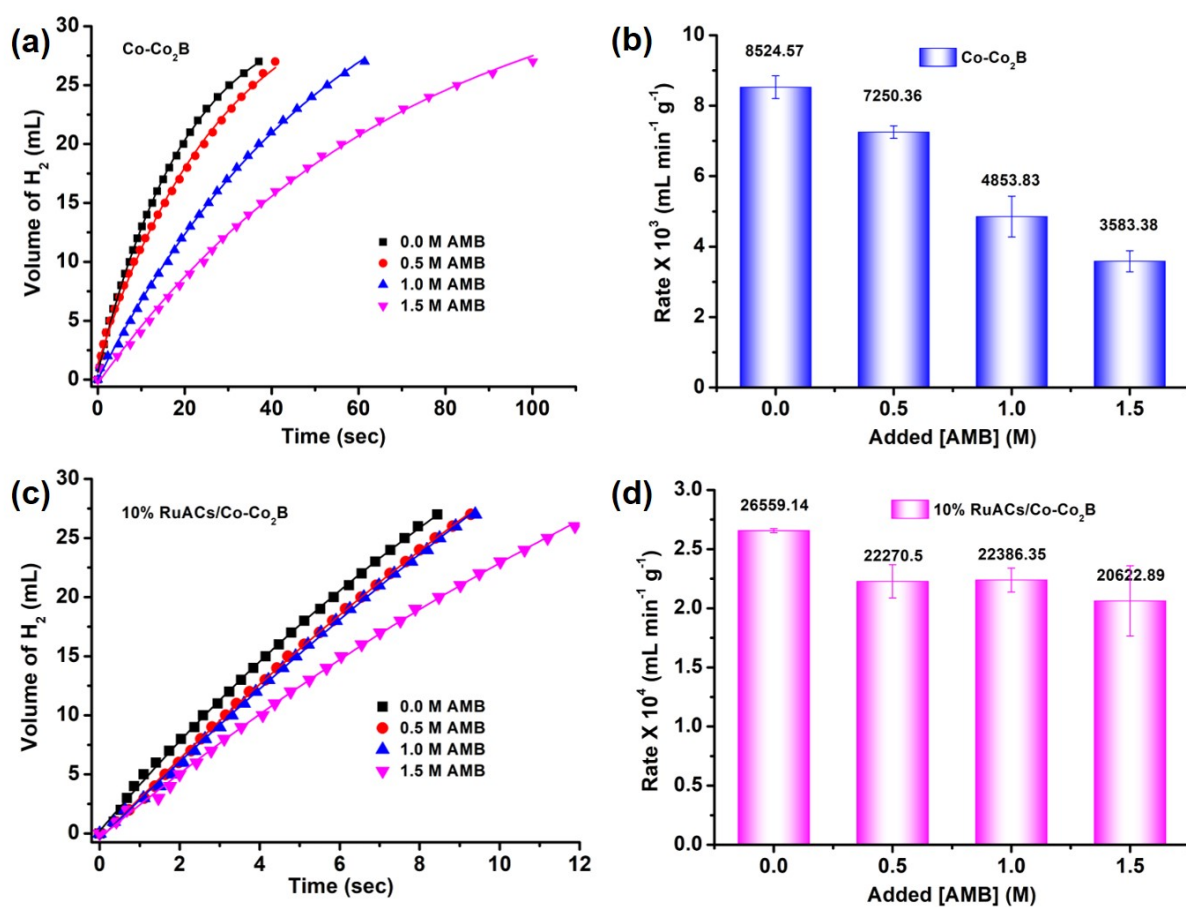
**Figure S12:** (a) Effect of externally added AMB inhibitor on the AB dehydrogenation by Co-Co$_2$B, (b) rate of AB dehydrogenation by Co-Co$_2$B corresponding to plots shown in (a), (c) effect of externally added AMB inhibitor on the AB dehydrogenation by 10% RuACs/Co-Co$_2$B, and (d) rate of AB dehydrogenation by 10% RuACs/Co-Co$_2$B corresponding to plots shown in (c).

**(a) Ru-13-atoms cluster**   **(b) Ru-19-atoms cluster**   **(c) Co$_2$B (211) facet**

**(d) Ru (002) facet**   **(e) Ru$_{19}$-Co$_2$B**

● Ru   ● Co   ● B
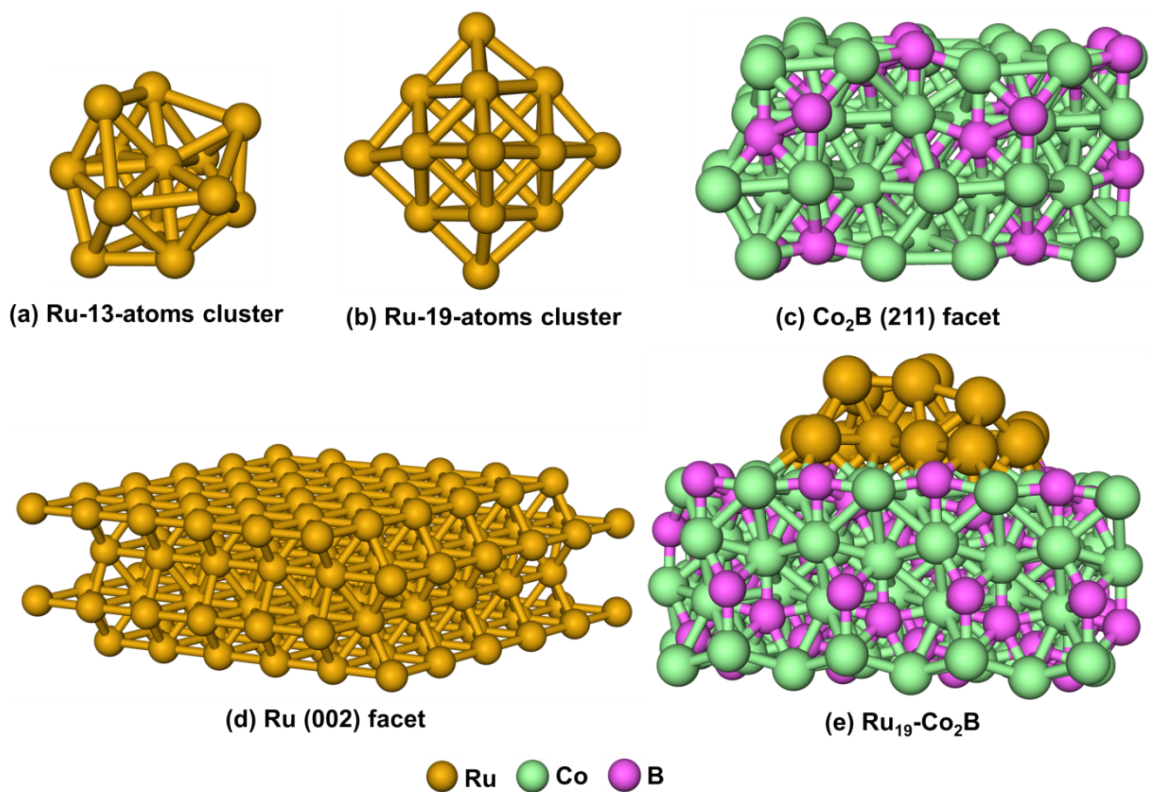
**Figure S13:** Structural snapshot of the selected catalyst systems (a) Ru$_{13}$-cluster, (b) Ru$_{19}$-cluster, (c) clean Co$_2$B (211) facet, (d) Ru (002) facet, (e) Ru-Co$_2$B for AB methanolysis with PBE-D3functional.

(a) (H$_3$NBH$_3$ + MeOH)@Ru (002)

(b) (H$_3$NBH$_2$(OMe) + MeOH)@Ru (002)

(c) (H$_3$NBH(OMe)$_2$ + MeOH)@Ru (002)

(d) (H$_3$NB(OMe)$_3$ + MeOH)@Ru (002)

Ru   B   C   H   N   O
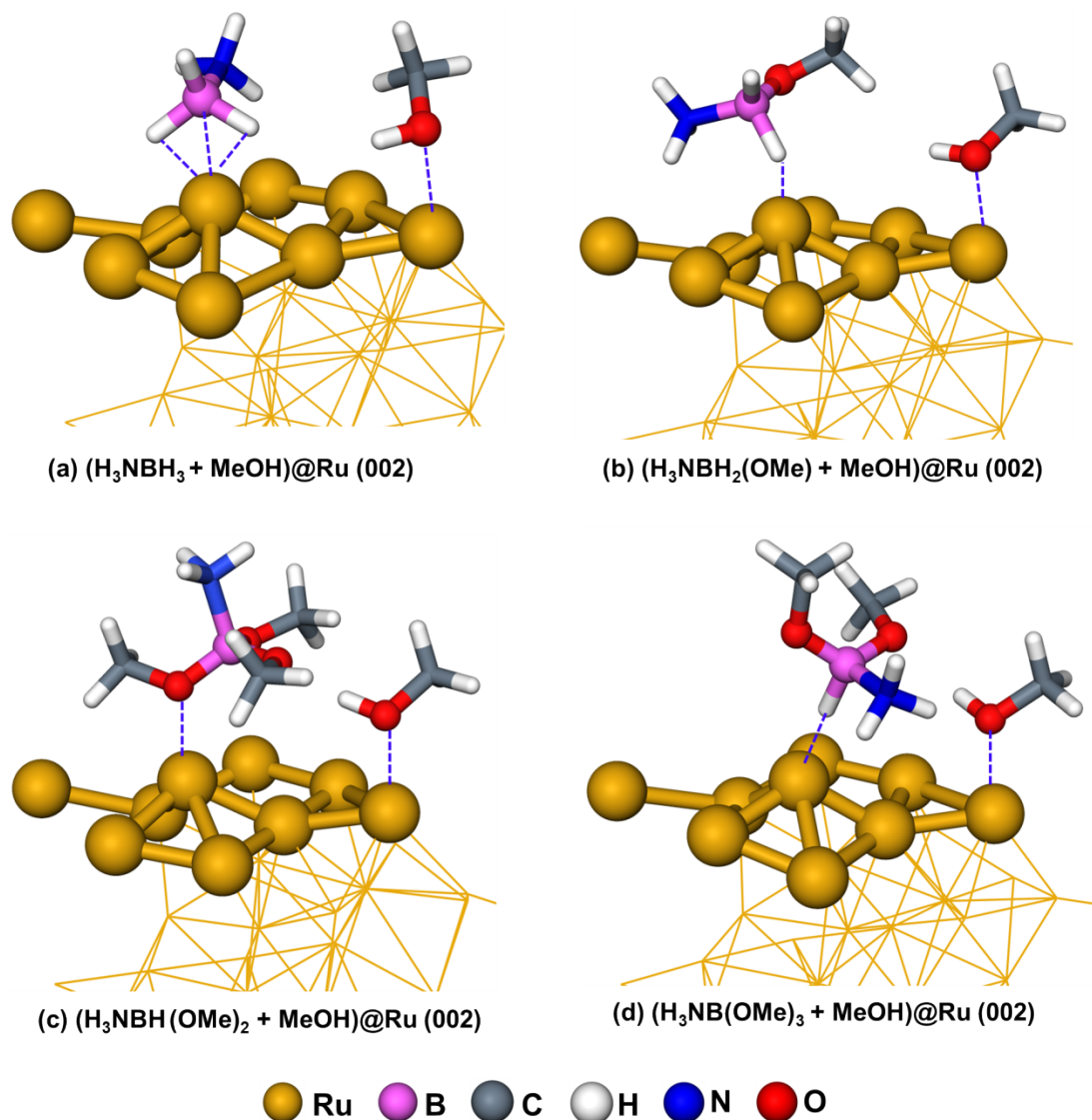
**Figure S14.** Close-up view of (a) AB, and 1st MeOH adsorption, (b) co-product (NH$_4$BH$_2$(OMe)) and 2nd MeOH interaction, (c) NH$_4$BH(OMe)$_2$ and 3rd MeOH interaction, (d) NH$_4$B(OMe)$_3$ and 4th MeOH interaction with Ru (002) facet using PBE-D3 functional.
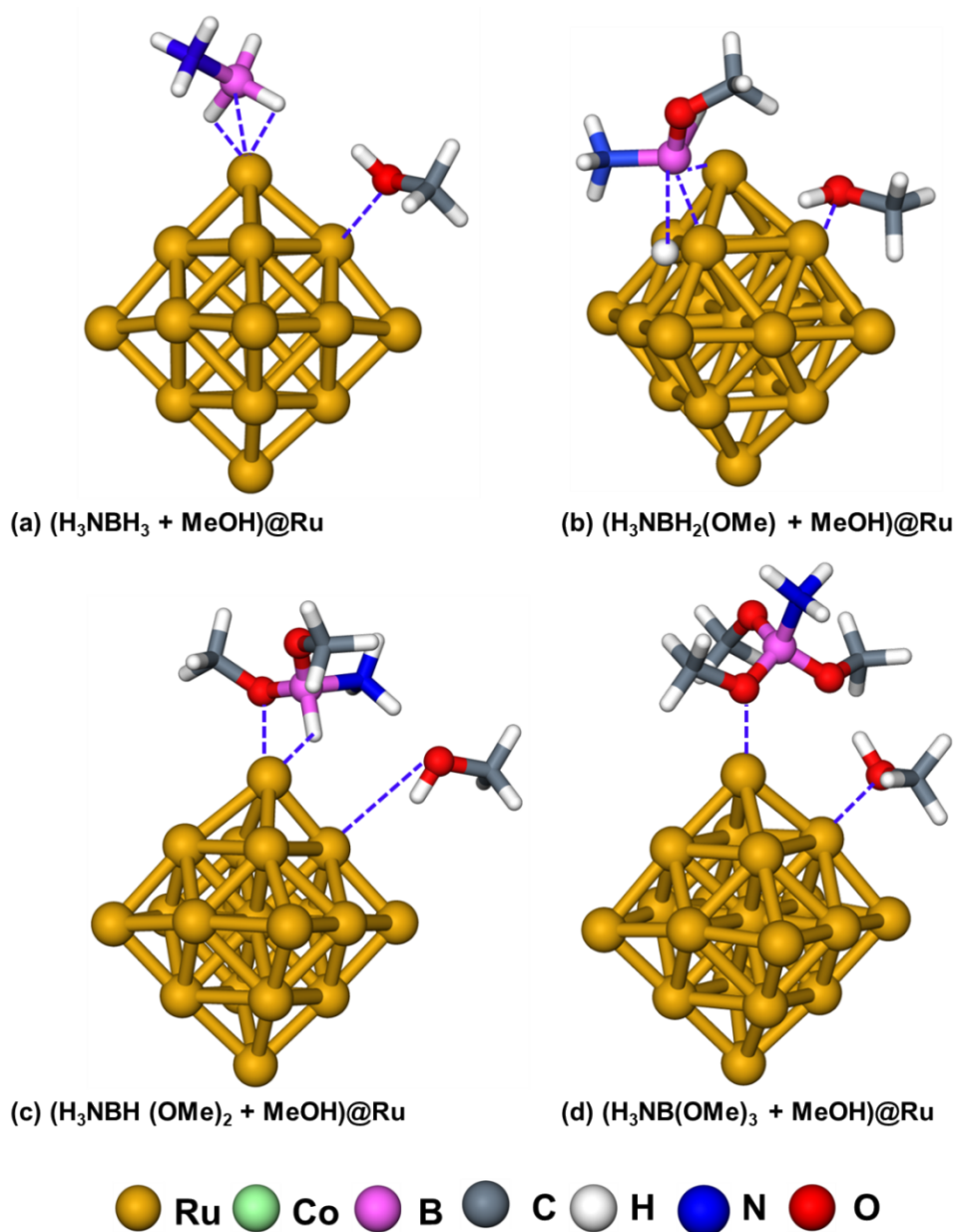
**Figure S15:** Structural snapshots of (a) AB, and 1st MeOH adsorption, (b) co-product (NH$_4$BH$_2$(OMe)) and 2nd MeOH interaction, (c) NH$_4$BH(OMe)$_2$ and 3rd MeOH interaction, (d) NH$_4$B(OMe)$_3$ and 4th MeOH interaction with Ru$_{19}$-cluster using PBE-D3 functional.
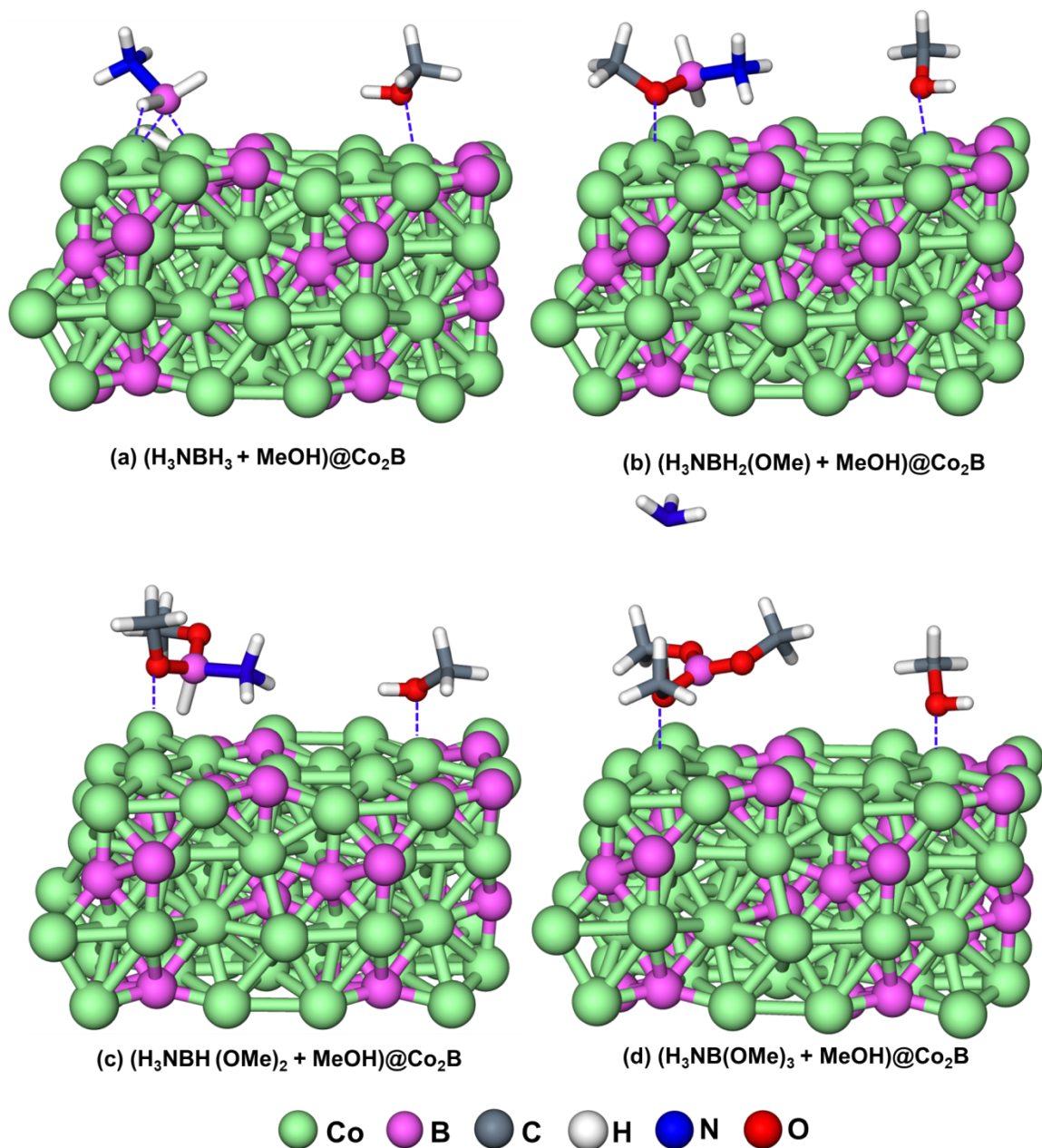
**Figure S16.** Snapshots to represent (a) AB, and $1^{st}$ MeOH adsorption, (b) co-product ($NH_4BH_2(OMe)$) and $2^{nd}$ MeOH interaction, (c) $NH_4BH(OMe)_2$ and $3^{rd}$ MeOH interaction, (d) $NH_4B(OMe)_3$ and $4^{th}$ MeOH interaction with clean $Co_2B$ (211) surface using PBE-D3 functional.
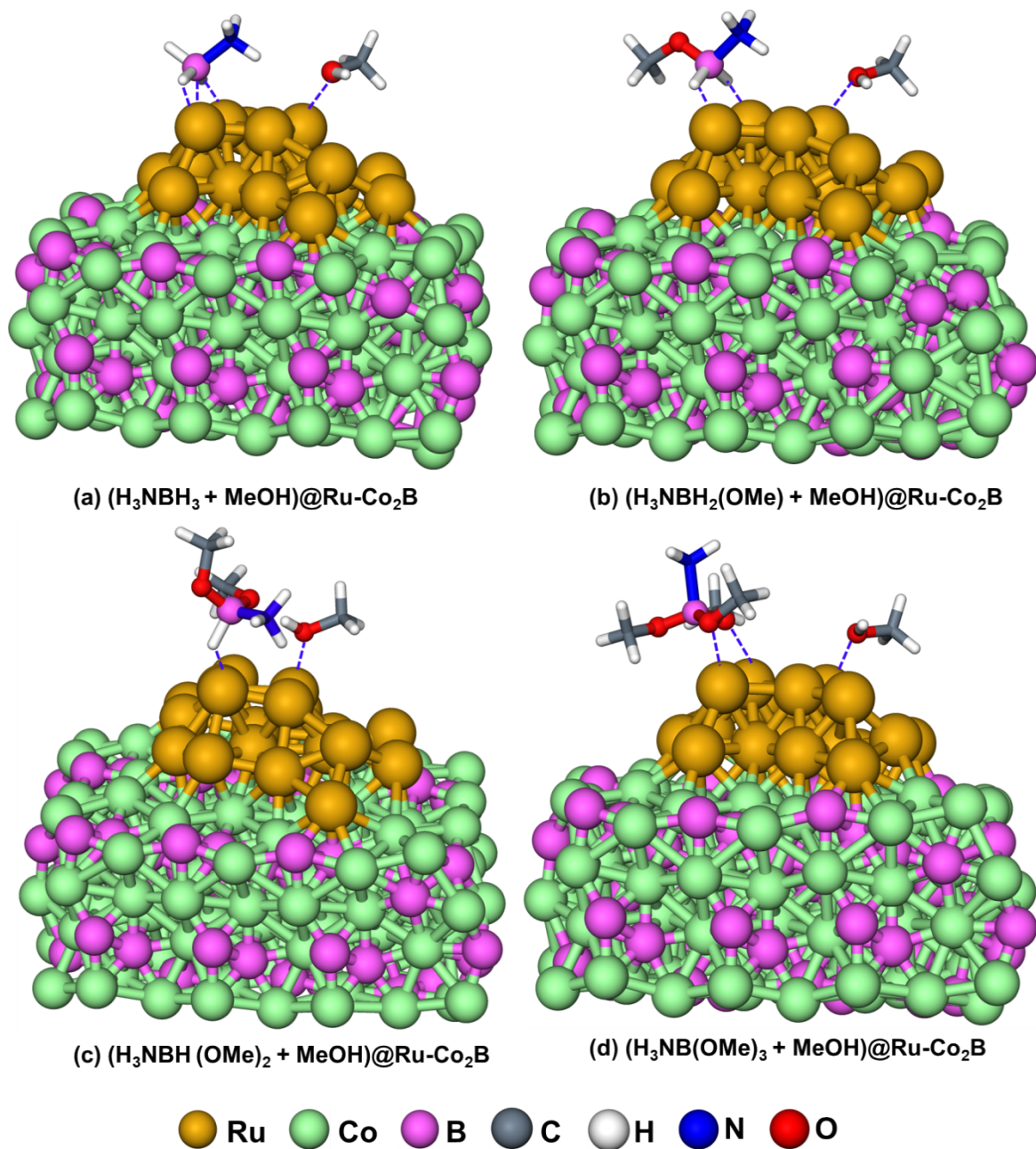
**Figure S17.** Structural snapshot of AB, MeOH, and co-product $(NH_4B(OMe)_x)$ interaction with Ru-Co$_2$B composite during (a) 1st MeOH adsorption step, (b) 2nd MeOH adsorption step, (c) 3rd MeOH adsorption step, (d) 4th MeOH adsorption step with PBE-D3 functional.
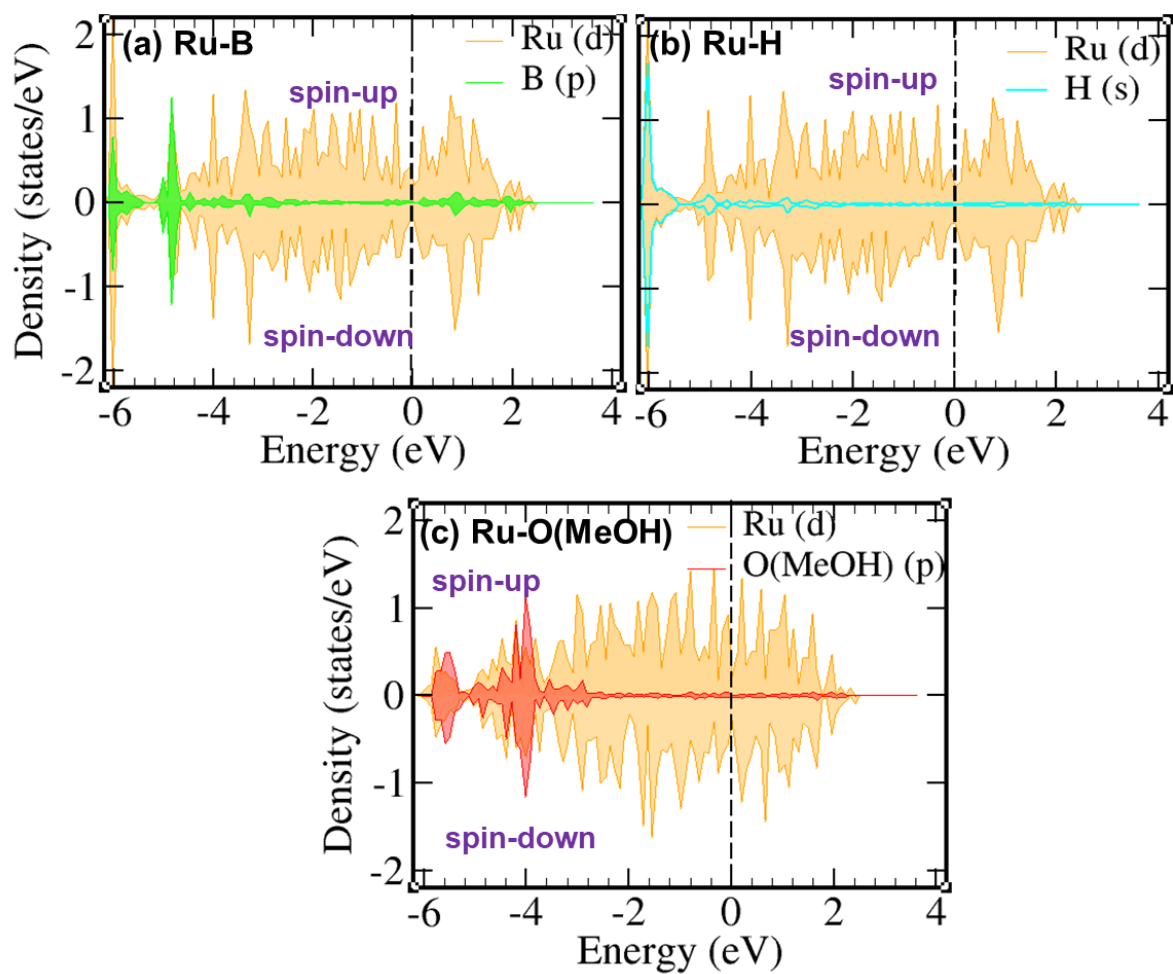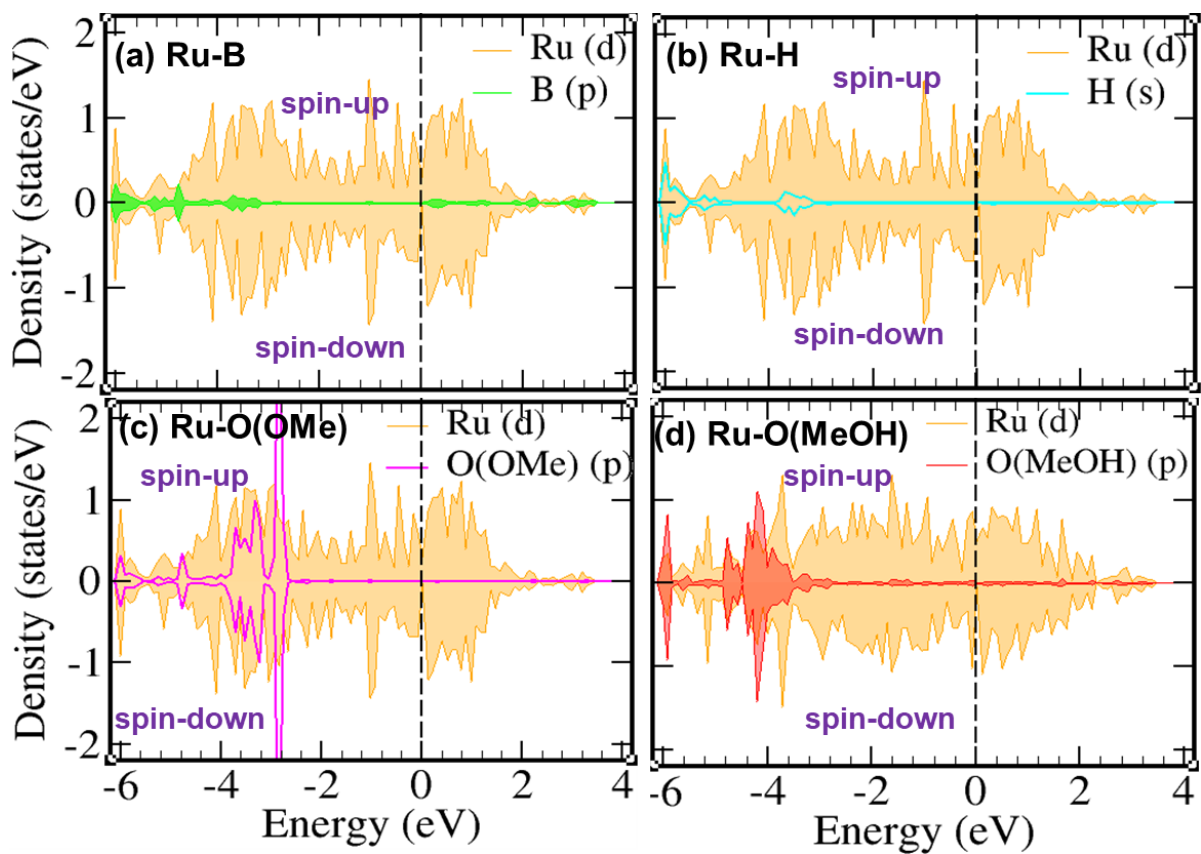
**Figure S18.** Atom projected density of states for (a) Ru-d- and B-p-bands, (b) Ru-d- and H-s-bands, (c) Ru-d- and O (MeOH)-p-bands during 1$^{st}$ MeOH and AB adsorption on Ru (002) facet using GGA functional.
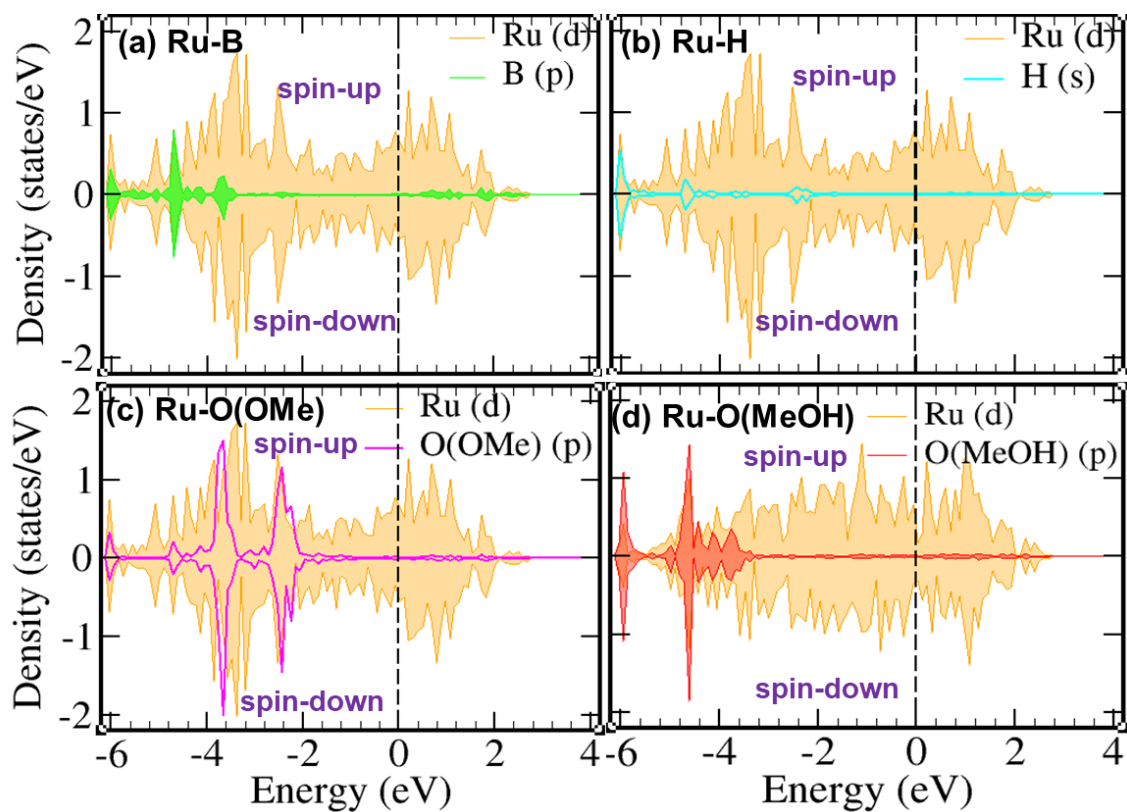
**Figure S19.** Atom projected density of states for (a) Ru-d- and B-p-bands, (b) Ru-d- and H-s-bands, (c) Ru-d- and O (OMe)-p-bands, and (d) Ru-d- and O (MeOH)-p-bands in the 2nd MeOH of AB on Ru (002) facet using GGA functional.
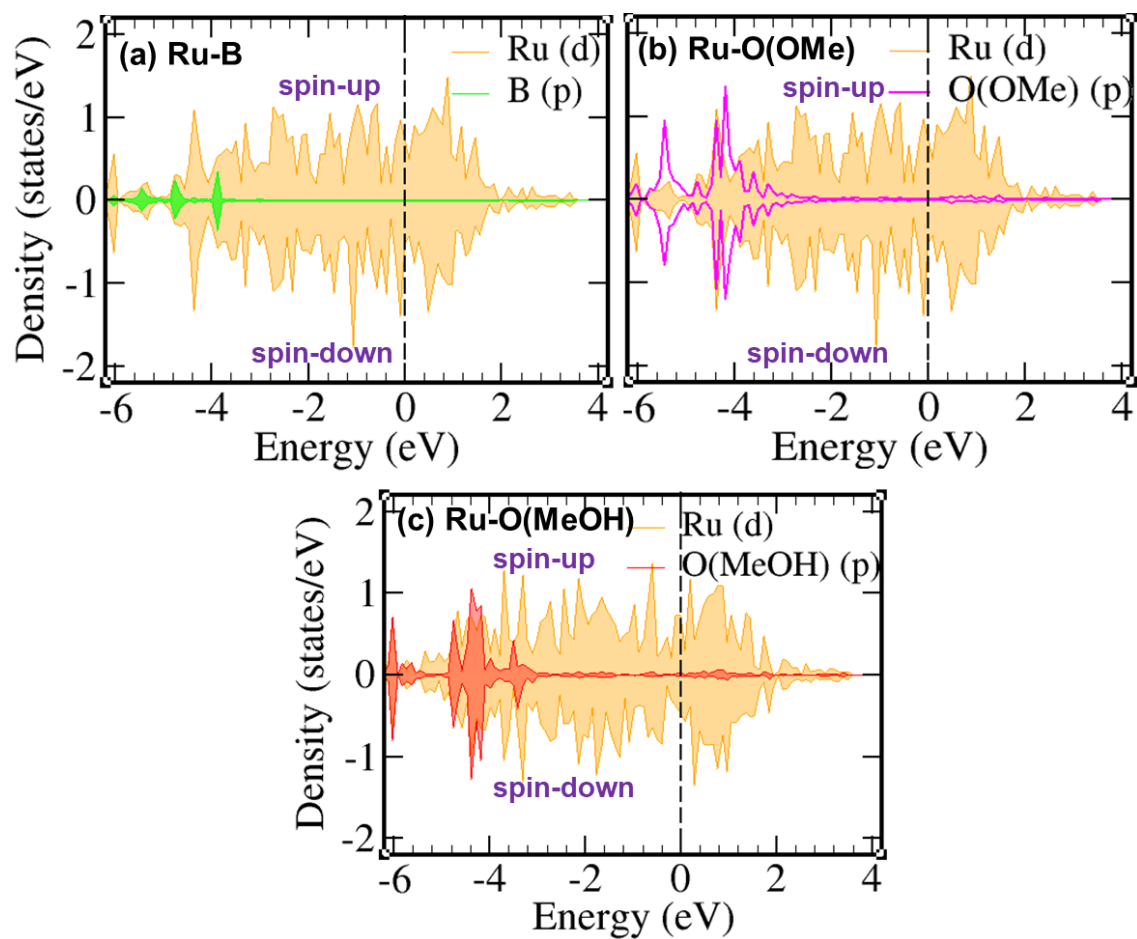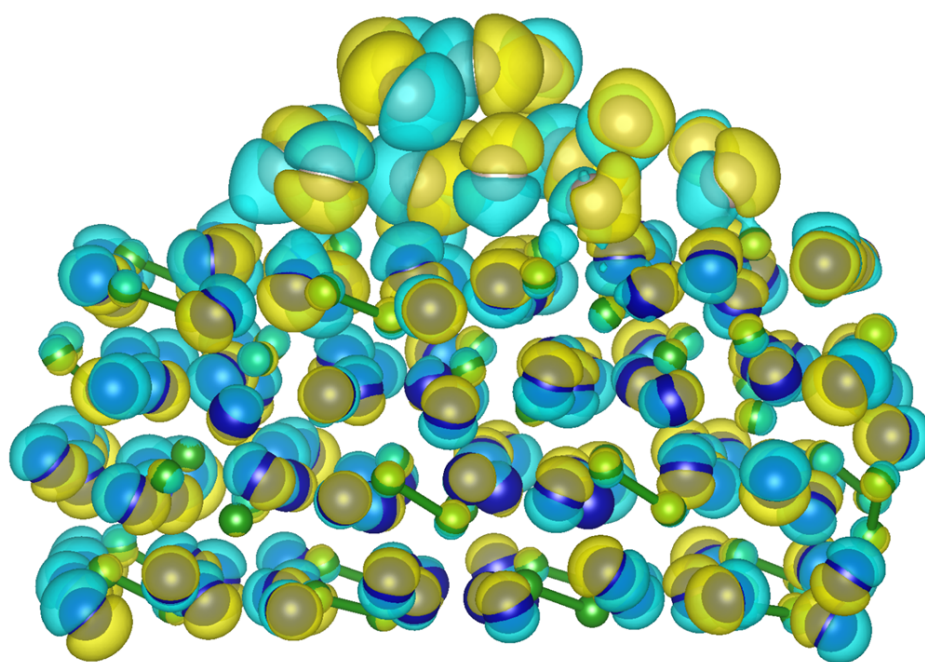
**Figure S20.** Atom projected density of states for (a) Ru-d- and B-p-bands, (b) Ru-d- and H-s-bands, (c) Ru-d- and O (OMe)-p-bands, and (d) Ru-d- and O (MeOH)-p-bands in the 3rd methanolysis of AB on Ru (002) facet using GGA functional.
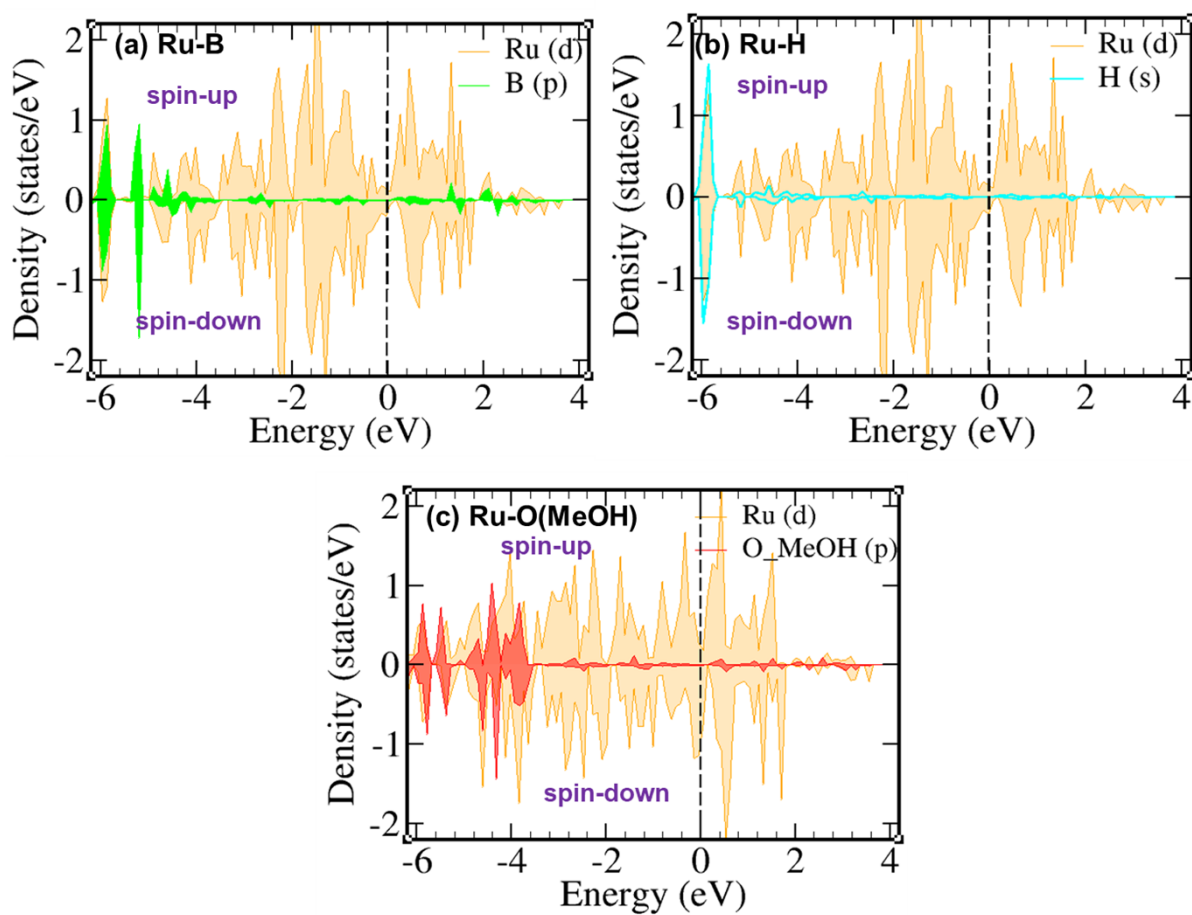
**Figure S21.** Atom projected density of states for (a) Ru-d- and B-p-bands, (b) Ru-d- and O (OMe)-p-bands, and (c) Ru-d- and O (MeOH)-p-bands in the 4th methanolysis of AB on Ru (002) facet using GGA functional.

**Ru-Co$_2$B**

**Figure S22.** Screenshot to represents difference charge density (DCD) on Ru-Co$_2$B with isosurface value 0.03. Yellow isosurface shows the charge gain sites, blue isosurface represents a charge depleted sites. Green, blue, and gold color atoms represent boron, cobalt, and ruthenium atoms respectively.

**Figure S23.** Atom projected density of states for (a) Ru-d- and B-p-bands, (b) Ru-d- and H-s-bands, (c) Ru-d- and O (MeOH)-p-bands during 1$^{st}$ MeOH and AB adsorption on Ru$_{19}$-cluster using GGA functional.
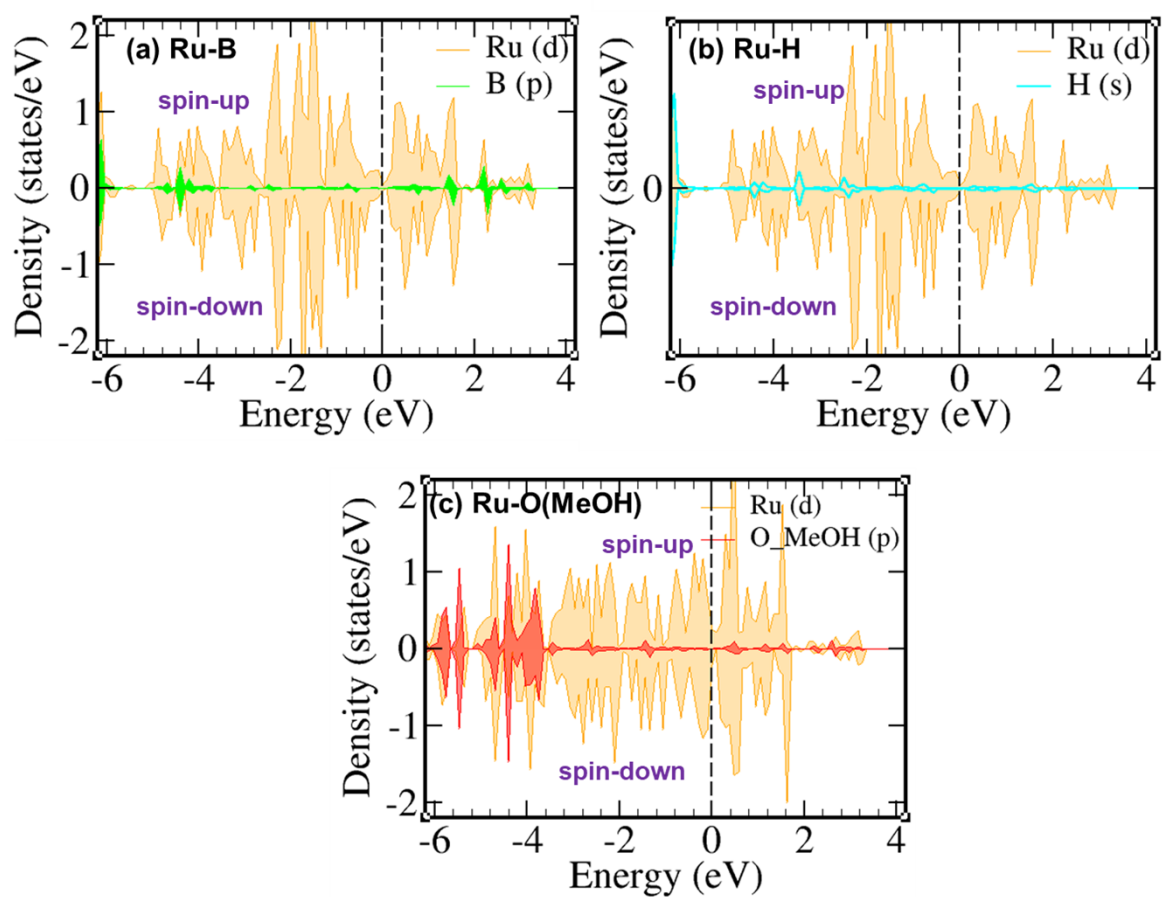
**Figure S24.** Atom projected density of states for (a) Ru-d- and B-p-bands, (b) Ru-d- and H-s-bands, (c) Ru-d- and O (MeOH)-p-bands in the 2nd methanolysis of AB on $Ru_{19}$-cluster using GGA functional.
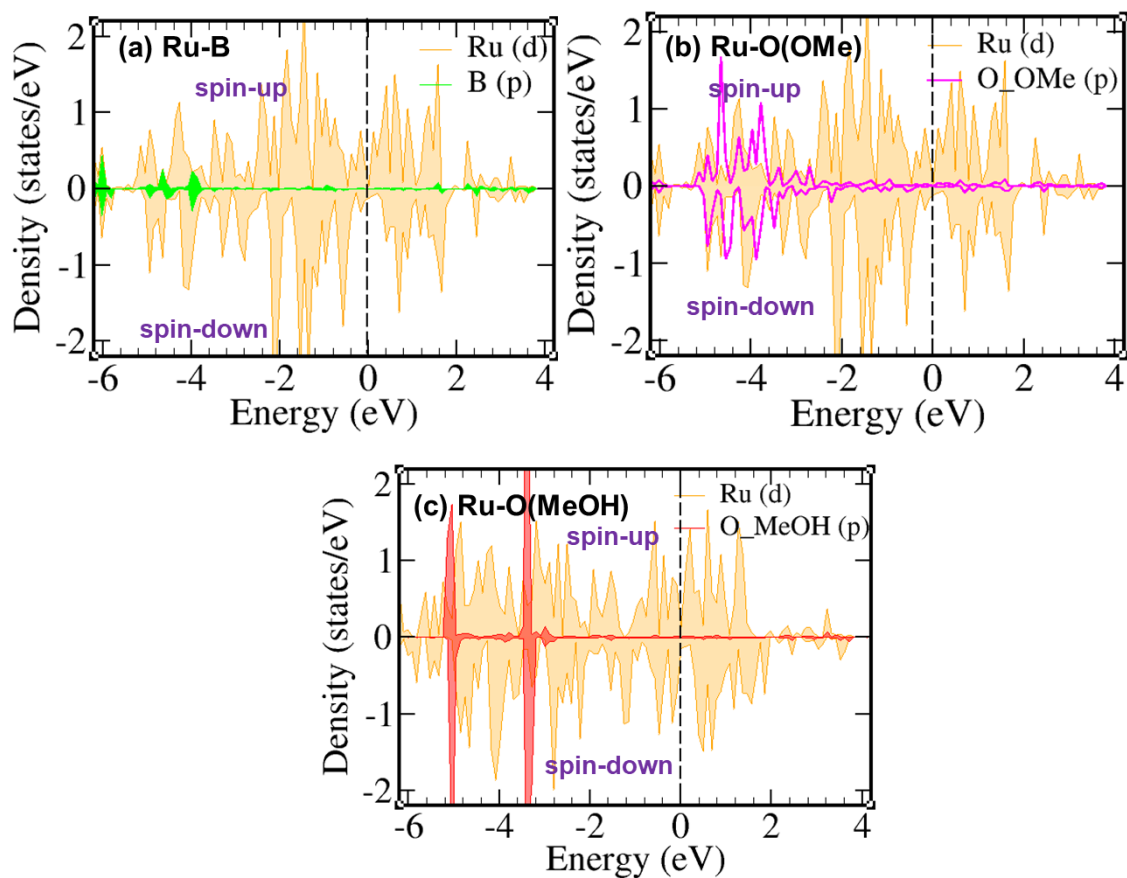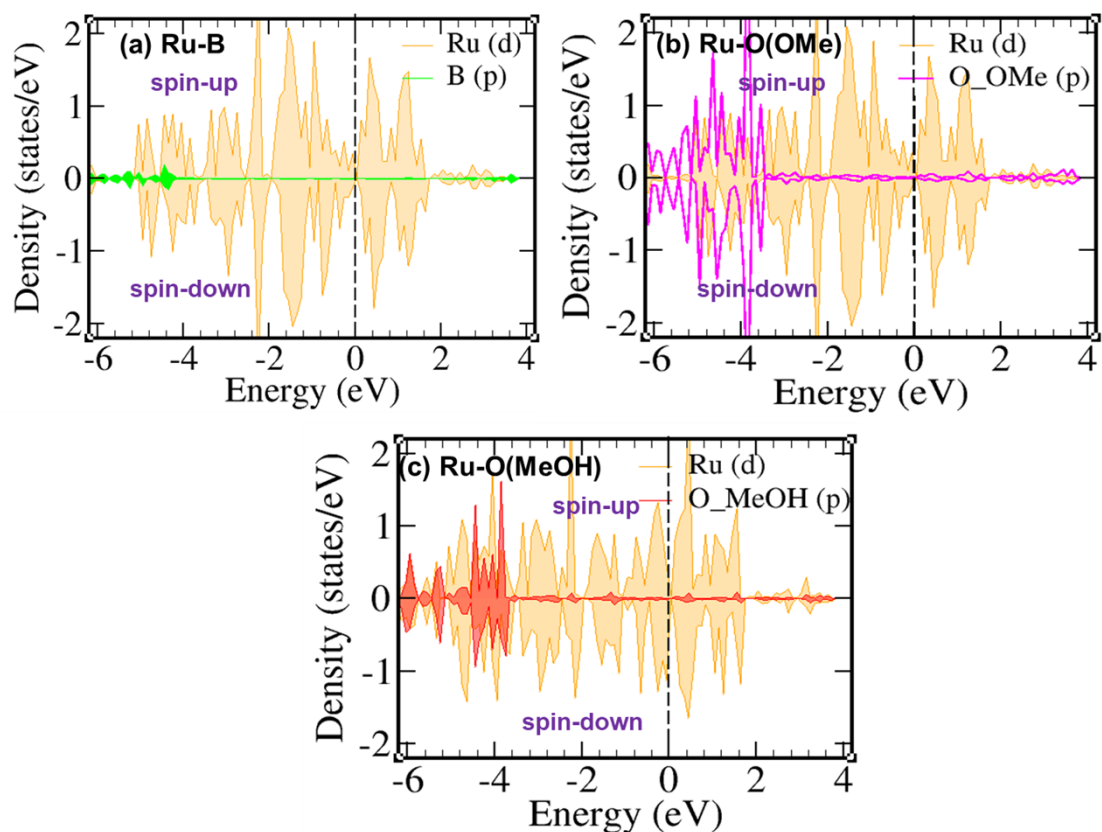
**Figure S25.** Atom projected density of states for (a) Ru-d- and B-p-bands, (b) Ru-d- and O (OMe)-p-bands, (c) Ru-d- and O (MeOH)-p-bands in the 3$^{rd}$ methanolysis of AB on Ru$_{19}$-cluster using GGA functional.

**Figure S26.** Atom projected density of states for (a) Ru-d- and B-p-bands, (b) Ru-d- and O (OMe)-p-bands, (c) Ru-d- and O (MeOH)-p-bands in the 4$^{th}$ methanolysis of AB on Ru$_{19}$-cluster using GGA functional.
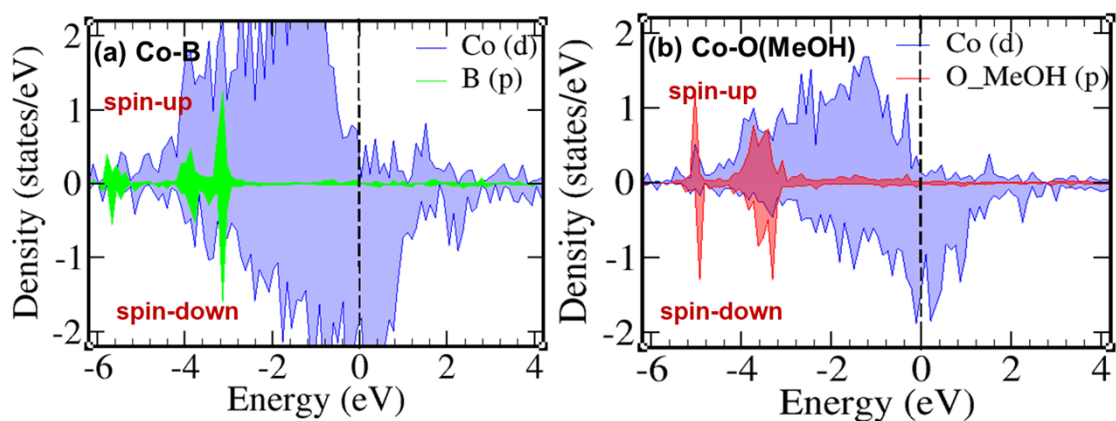


**Figure S27.** Atom projected density of states for (a) Co-d- and B-p-bands, and (b) Co-d- and O (MeOH)-p-bands during 1$^{st}$ MeOH and AB adsorption on clean Co$_2$B (211) surface using GGA functional.
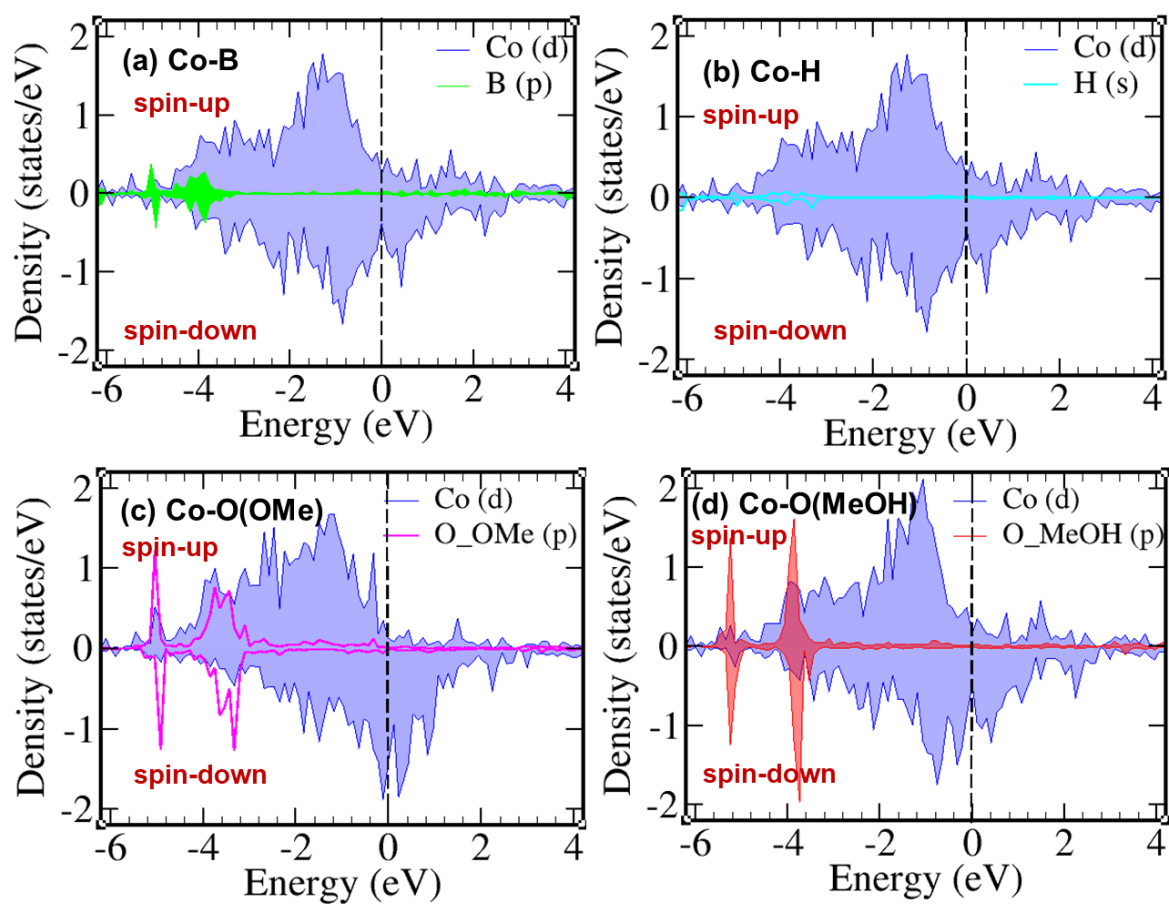
**Figure S28.** Atom projected density of states for (a) Co-d- and B-p-bands, (b) Co-d- and H-s-bands, (c) Co-d- and O (OMe)-p-bands, and (d) Co-d- and O (MeOH)-p-bands in the $2^{nd}$ methanolysis of AB on clean $Co_2B$ (211) surface using GGA functional.
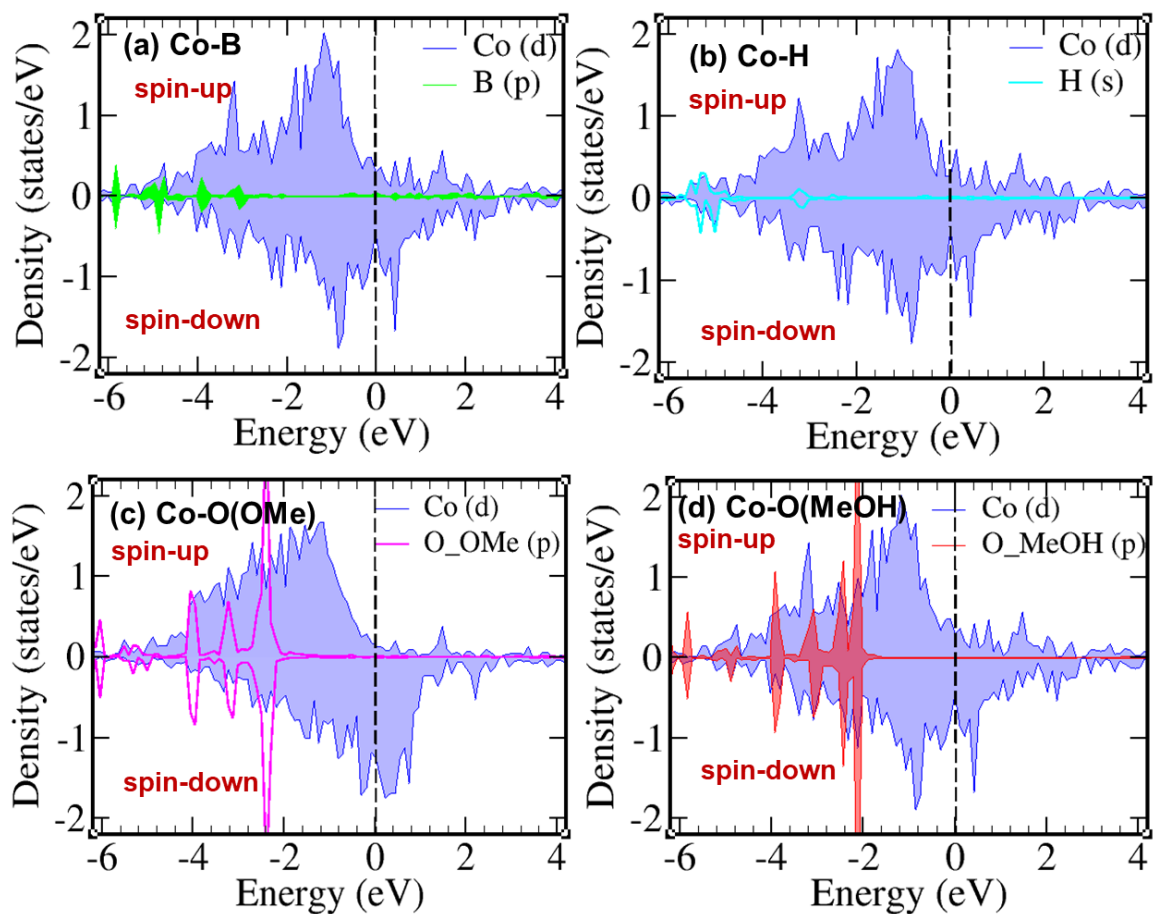
**Figure S29.** Atom projected density of states for (a) Co-d- and B-p-bands, (b) Co-d- and H-s-bands, (c) Co-d- and O (OMe)-p-bands, and (d) Co-d- and O (MeOH)-p-bands in the 3$^{rd}$ methanolysis of AB on clean Co$_2$B (211) surface using GGA functional.
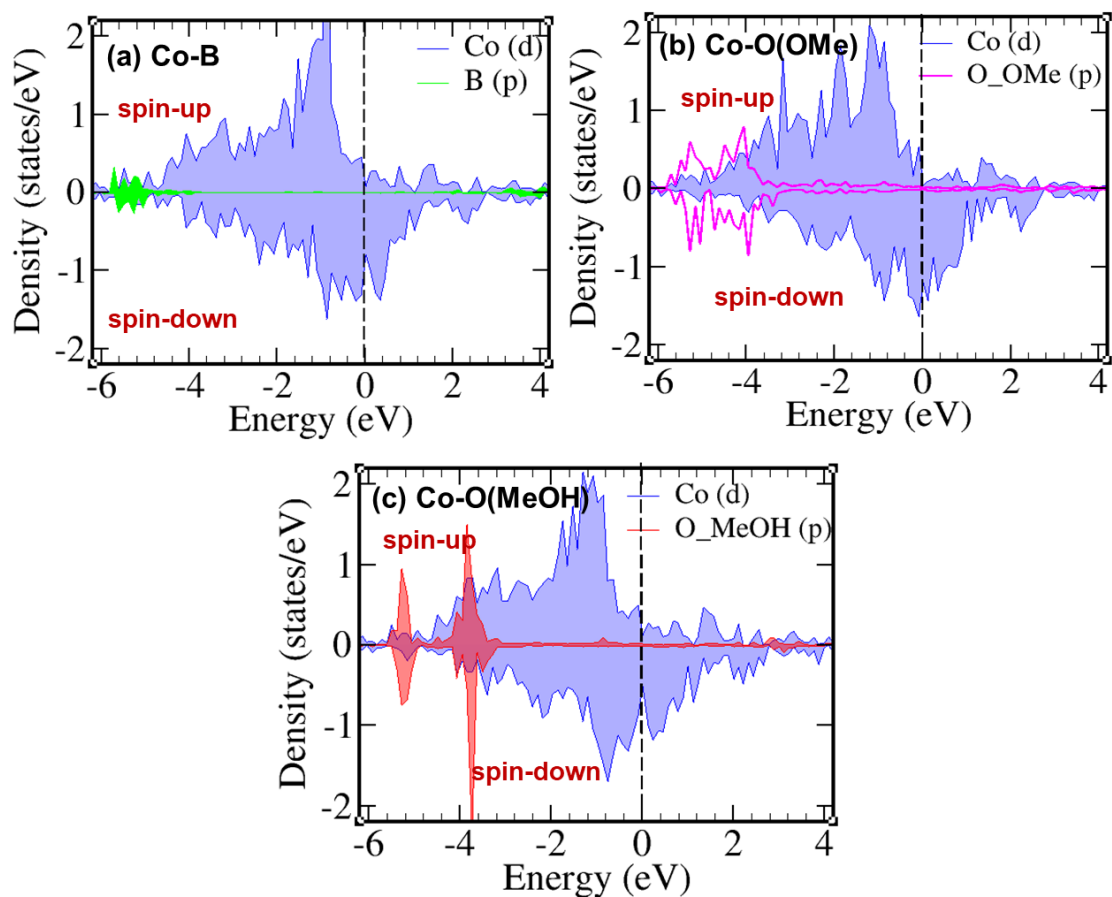
**Figure S30.** Atom projected density of states for (a) Co-d- and B-p-bands , (b) Co-d- and O (OMe)-p-bands , and (c) Co-d- and O (MeOH)-p-bands  in the $4^{th}$ methanolysis of AB on clean $Co_2B$ (211) surface using GGA functional.
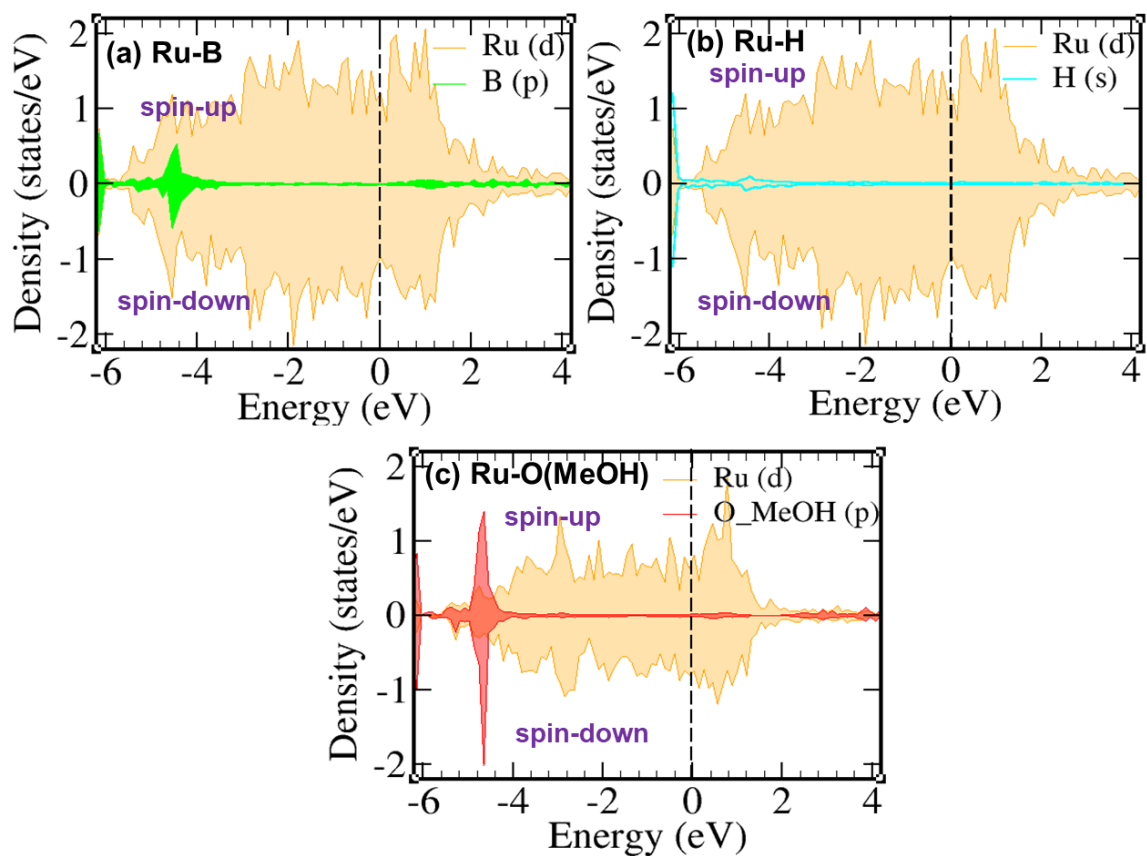
**Figure S31.** Atom projected density of states for (a) Ru-d- and B-p-bands, (b) Ru-d- and H-s-bands, (c) Ru-d- and O (MeOH)-p-bands during 1st MeOH and AB adsorption on Ru-Co$_2$B using GGA functional.
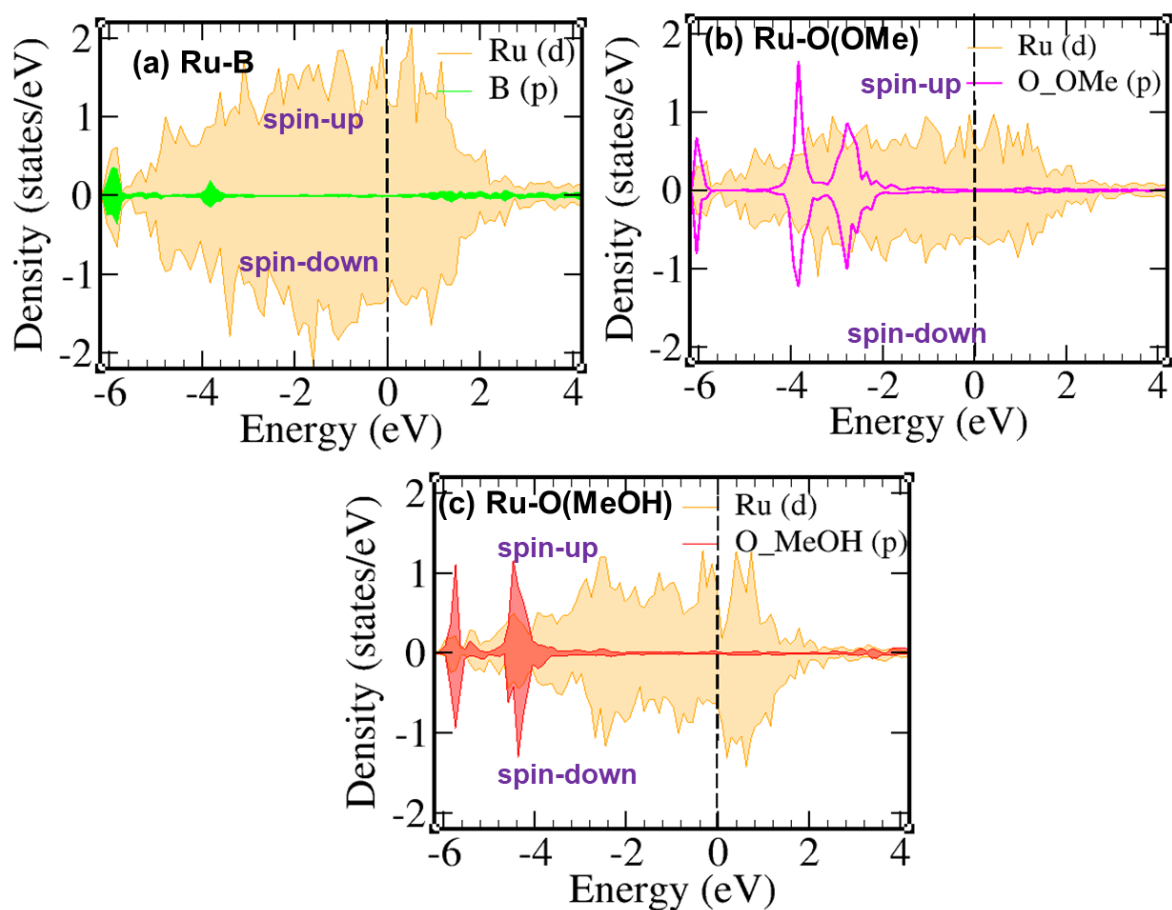
**Figure S32.** Atom projected density of states for (a) Ru-d- and B-p-bands, (b) Ru-d- and O (OMe)-p-bands, (c) Ru-d- and O (MeOH)-p-bands in the 2$^{nd}$ methanolysis of AB on Ru-Co$_2$B using GGA functional.

**Figure S33.** Atom projected density of states for (a) Ru-d- and B-p-bands, (b) Ru-d- and O (OMe)-p-bands, and (c) Ru-d- and O (MeOH)-p-bands in the 3$^{rd}$ methanolysis of AB on Ru-Co$_2$B using GGA functional.
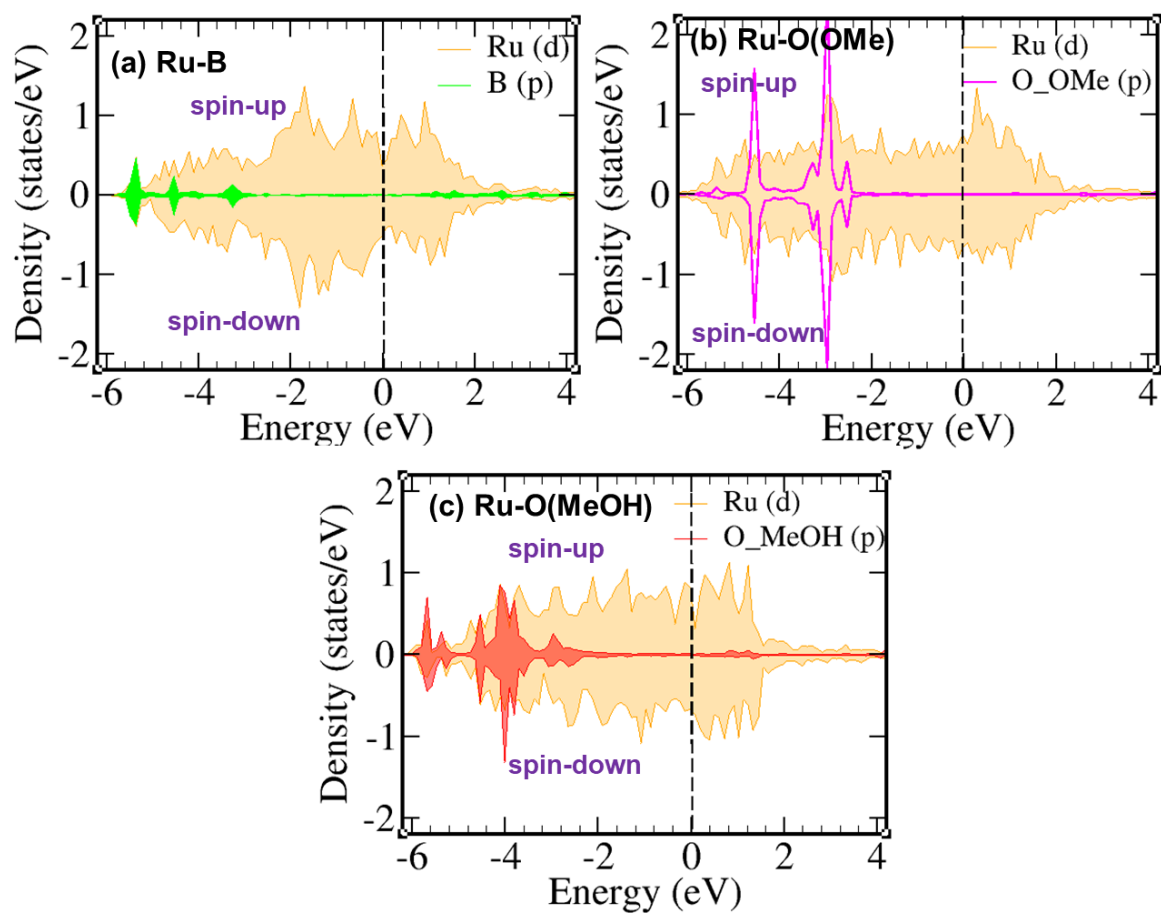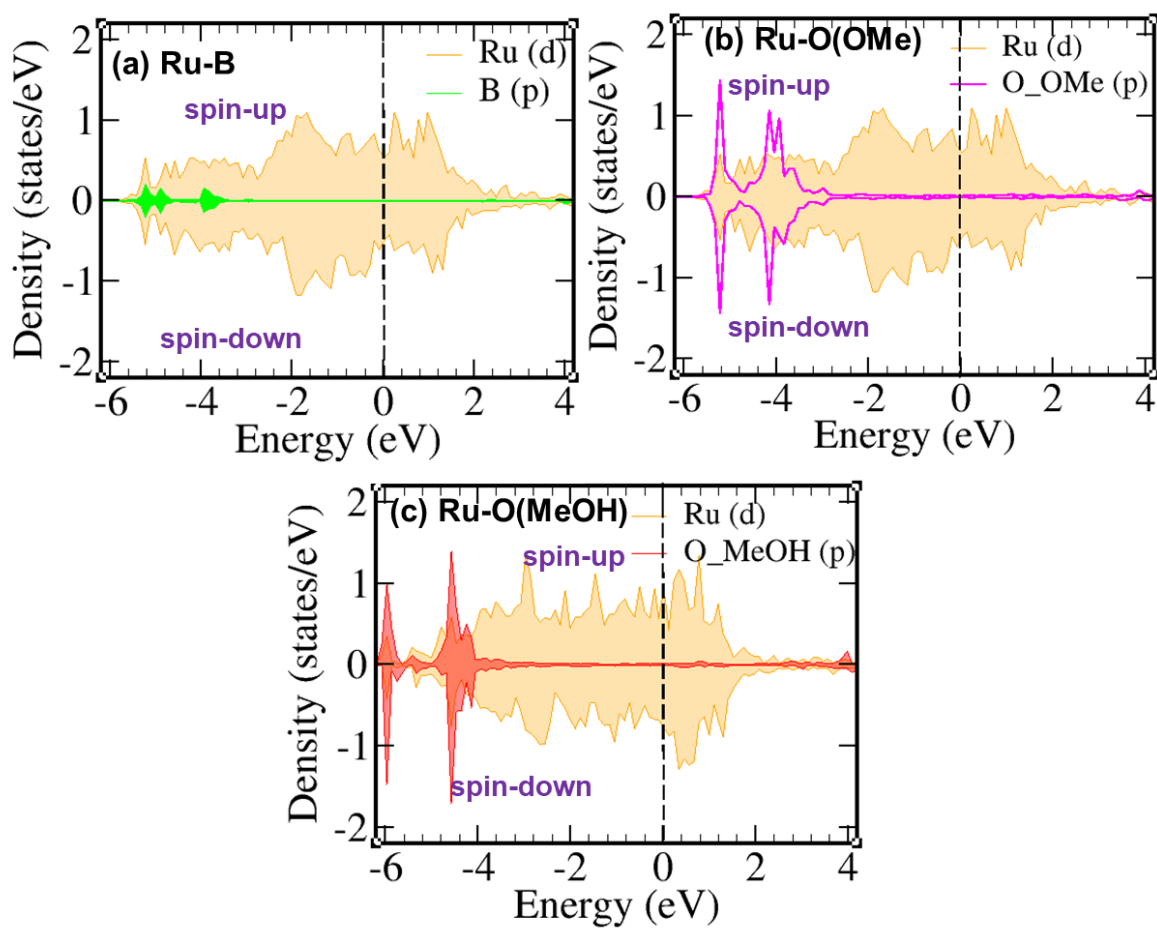
**Figure S34.** Atom projected density of states for (a) Ru-d- and B-p-bands, (b) Ru-d- and O (OMe)-p-bands, and (c) Ru-d- and O (MeOH)-p-bands in the 4th methanolysis of AB on Ru-$Co_2B$ using GGA functional.
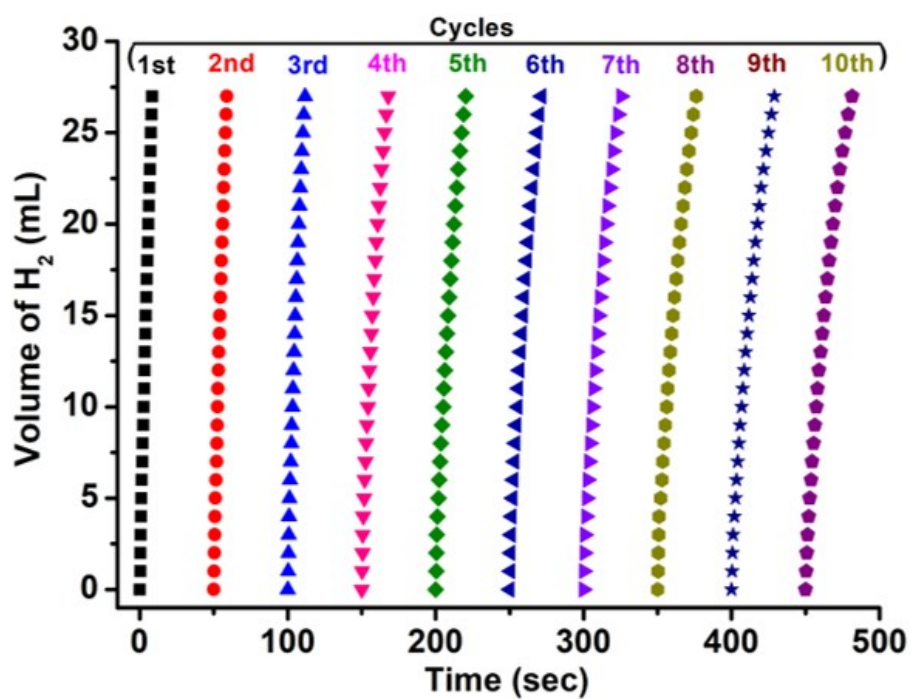
**Figure S35:** (a) Reusability studies of 10% RuACs/Co-Co$_2$B catalyst.
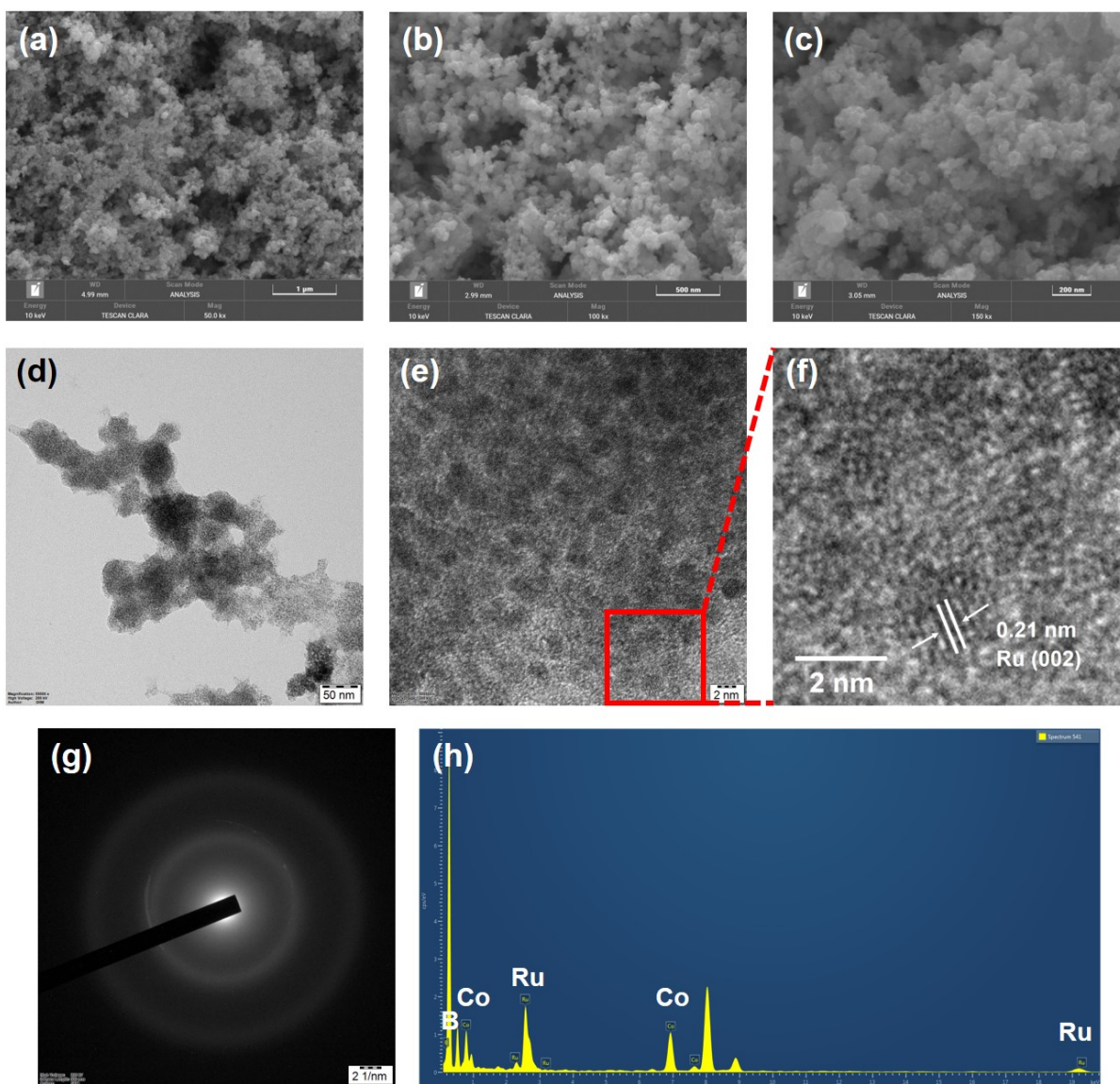
**Figure S36:** Characterization of 10% RuACs/Co-Co$_2$B catalyst recovered after 10$^{th}$ cycle (a-c) SEM images at different magnifications, (d) TEM images, (e) HRTEM image, (f) magnified portion of the selected area from (e) showing lattice fringes of Ru, (g) SAED pattern, and (h) EDX spectra.

**Figure S37:** Comparison of methanolysis and hydrolysis of AB catalyzed by 10% RuACs/Co-Co$_2$B and inset shows the result of the phenolphthalein test. The appearance of pink color indicates the release of ammonia during hydrolysis.

**Figure S38:** Comparison of AB dehydrogenation catalyzed by 10% RuACs/Co-Co$_2$B in methanol and deuterated methanol.
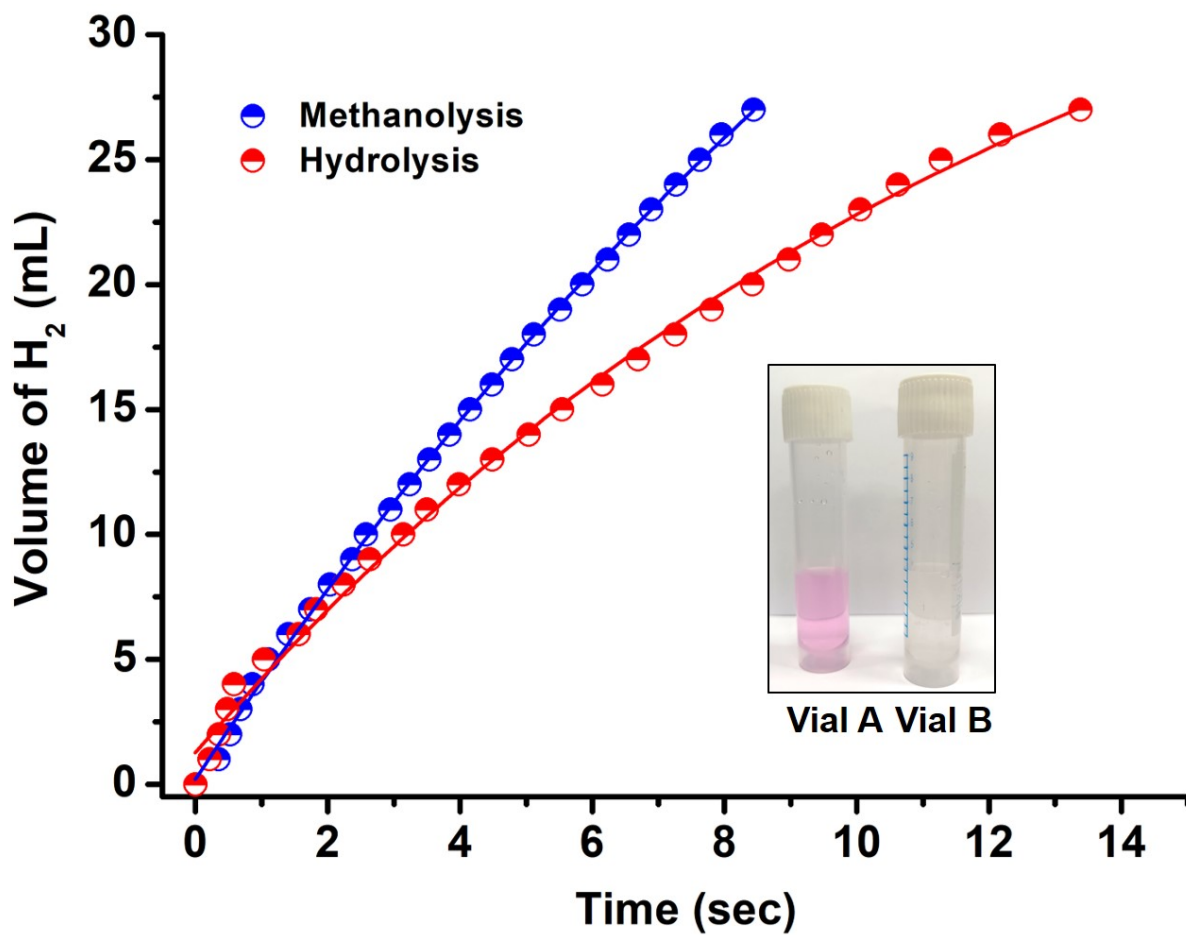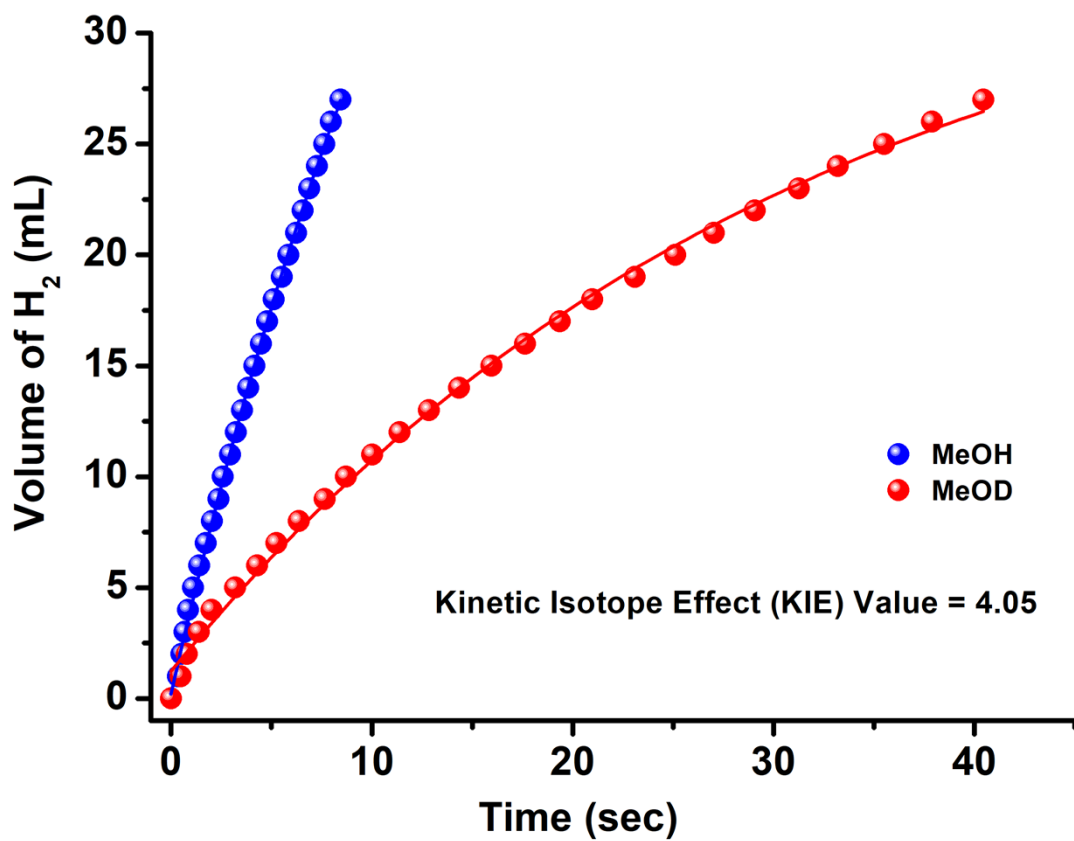
**Table S1:** AB Dehydrogenation reaction completion time for Co-Co$_2$B and 10% RuACs/Co-Co$_2$B.

| Catalyst | 1$^{st}$ half-life (sec) (50%) | 2$^{nd}$ half-life (sec) (75%) | 3$^{rd}$ half-life (sec) (87.5%) | 4$^{th}$ half-life (sec) (93.75%) |
|---|---|---|---|---|
| Co-Co$_2$B | 10.67 | 19.87 | 26.76 | 31.33 |
| 10% RuACs/Co-Co$_2$B | 3.67 | 5.89 | 7.13 | 7.78 |

**Table S2:** Difference between two successive half-lives for AB Dehydrogenation by Co-Co$_2$B and 10% RuACs/Co-Co$_2$B.

| Catalyst | 1$^{st}$ half-life (sec) (50%) | 2$^{nd}$ half-life (sec) (75%) | 3$^{rd}$ half-life (sec) (87.5%) | 4$^{th}$ half-life (sec) (93.75%) |
|---|---|---|---|---|
| Co-Co$_2$B | 10.67 | 9.2 | 6.89 | 4.57 |
| 10% RuACs/Co-Co$_2$B | 3.67 | 2.22 | 1.24 | 0.65 |

**Table S3:** Computed adsorption energy (ΔE) for AB adsorption on Ru clusters (Ru$_{13}$- and Ru$_{19}$-cluster), clean Co$_2$B (211) surface, Ru (002) surface, and Ru-Co$_2$B composites (Ru$_{19}$-Co$_2$B, Ru$_{13}$-Co$_2$B)

| Catalysts | Adsorption Energy (ΔE) (kcal/mol) | | | |
|---|---|---|---|---|
| | **1$^{st}$ MeOH adsorption** | **2$^{nd}$ MeOH adsorption** | **3$^{rd}$ MeOH adsorption** | **4$^{th}$ MeOH adsorption** |
| Ru$_{13}$-cluster | -44.311 | -60.490 | -61.113 | -74.978 |
| Ru$_{19}$-cluster | -41.601 | -51.666 | -63.113 | -73.365 |
| Ru (002) facet | -129.359 | -111.193 | -129.208 | -183.969 |
| Co$_2$B (211) facet | -67.459 | -71.887 | -73.689 | -89.905 |
| Ru$_{19}$-Co$_2$B (211) | -46.227 | -56.846 | -67.908 | -80.817 |
| Ru$_{13}$-Co$_2$B (211) | -50.198 | -60.227 | -64.789 | -81.234 |

**Table S4:** Computed bond distances for Ru-B, Ru-O (OMe), Co-O (OMe), and Co-B bonds in the case of Ru$_{19}$-cluster, clean Co$_2$B and Ru-Co$_2$B composite (at different methanolysis steps).

| | Ru$_{19}$-cluster | | |
|:---:|:---:|:---:|:---:|
| **Ru-B (Å)** | **Ru-O1 (OMe) (Å)** | **Ru-O2 (OMe) (Å)** | **Ru-O3 (OMe) (Å)** |
| 2.257 | - | - | - |
| 2.193 | 3.595 | - | - |
| 2.425 | 2.254 | 3.595 | |
| 3.183 | 2.171 | 3.165 | 4.084 |
| | **Co$_2$B (211)** | | |
| **Co-B (Å)** | **Co-O1 (OMe) (Å)** | **Co-O2 (OMe) (Å)** | **Co-O3 (OMe) (Å)** |
| 2.168 | - | - | - |
| 2.557 | 2.001 | - | - |
| 2.796 | 2.735 | 3.821 | - |
| 2.487 | 2.008 | 2.293 | 2.009 |
| | **Ru-Co$_2$B** | | |
| **Ru-B (Å)** | **Ru-O1 (OMe) (Å)** | **Ru-O2 (OMe) (Å)** | **Ru-O3 (OMe) (Å)** |
| 2.585 | - | - | - |
| 2.541 | 3.680 | - | - |
| 3.181 | 3.971 | 4.017 | - |
| 3.206 | 2.321 | 2.379 | 3.649 |

**Table S5:** Comparison of catalytic activities of some reported Co-Ru alloy and Ru based catalysts for AB dehydrogenation.

| Catalysts | TOF ($mol_{H_2} \, mol^{-1}_{(Ru)} min^{-1}$) | Solvent | Ref. |
|---|---|---|---|
| CoRu$_{0.5}$/CQDs | 3255.4 | Water | Li et al.[10] |
| Ru$_1$Co$_1$@MIL-96 | 320.7 | Water | Lu et al.[11] |
| Ru$_1$Co$_9$/TiO$_2$ | 1408 | Water | Zhang et al.[12] |
| Ru$_{0.075}$Co$_{0.925}$/NPC | 2590 | Water | Li et al.[13] |
| Ru/TiO$_2$ P25 | 604 | Water | Mori et al.[14] |
| Ru$^0$ /CeO$_2$ | 361 | Water | Akbayrak et al.[15] |
| Ru/SAPO-34-0.8Si (Si/Al = 0.8) | 490 | Water | Sun et al.[16] |
| Ru/FAU (Si/Al = 30) | 627 | Water | Sun et al.[16] |
| Ru/PCC-2 | 304.4 | MeOH | Fang et al.[17] |
| Ru(0)@MWCNT | 329 | Water | Akbayrak et al.[18] |
| **10% RuACs/Co-Co$_2$B** | **1032.2 ± 114.6** | **MeOH** | **This work** |

## References

[1]     P. V. Ramachandran, P. D. Gagare, *Inorg. Chem.* **2007**, *46*, 7810–7817.

[2]     X. Wang, L. Zhang, H. Lin, Q. Nong, Y. Wu, T. Wu, Y. He, *Rsc Adv.* **2014**, *4*, 40029–40035.

[3]     G. Kresse, J. Furthmüller, *Phys. Rev. B* **1996**, *54*, 11169.

[4]     G. Kresse, J. Hafner, *Phys. Rev. B* **1993**, *47*, 558.

[5]     J. P. Perdew, K. Burke, M. Ernzerhof, *Phys. Rev. Lett.* **1996**, *77*, 3865.

[6]     J. VandeVondele, M. Krack, F. Mohamed, M. Parrinello, T. Chassaing, J. Hutter, *Comput. Phys. Commun.* **2005**, *167*, 103–128.

[7]     S. Grimme, J. Antony, S. Ehrlich, H. Krieg, *J. Chem. Phys.* **2010**, *132*.

[8]     R. Dronskowski, P. E. Blöchl, *J. Phys. Chem.* **1993**, *97*, 8617–8624.

[9]     V. L. Deringer, A. L. Tchougréeff, R. Dronskowski, *J. Phys. Chem. A* **2011**, *115*, 5461–5466.

[10]    W. Li, Y. Zhao, Y. Liu, M. Sun, G. I. N. Waterhouse, B. Huang, K. Zhang, T. Zhang, S. Lu, *Angew. Chemie Int. Ed.* **2021**, *60*, 3290–3298.

[11]    D. Lu, G. Yu, Y. Li, M. Chen, Y. Pan, L. Zhou, K. Yang, X. Xiong, P. Wu, Q. Xia, *J. Alloys Compd.* **2017**, *694*, 662–671.

[12]    J. Zhang, J. Li, L. Yang, R. Li, F. Zhang, H. Dong, *Int. J. Hydrogen Energy* **2021**, *46*, 3964–3973.

[13]    G. Li, N. Wei, Y. Wang, *Appl. Surf. Sci.* **2023**, *610*, 155459.

[14]    K. Mori, K. Miyawaki, H. Yamashita, *ACS Catal.* **2016**, *6*, 3128–3135.

[15]    S. Akbayrak, Y. Tonbul, S. Özkar, *Dalt. Trans.* **2016**, *45*, 10969–10978.

[16]    Q. Sun, N. Wang, R. Bai, Y. Hui, T. Zhang, D. A. Do, P. Zhang, L. Song, S. Miao, J. Yu, *Adv. Sci.* **2019**, *6*, 1802350.

[17]    Y. Fang, J. Li, T. Togo, F. Jin, Z. Xiao, L. Liu, H. Drake, X. Lian, H.-C. Zhou, *Chem* **2018**, *4*, 555–563.

[18]    S. Akbayrak, S. Özkar, *ACS Appl. Mater. Interfaces* **2012**, *4*, 6302–6310.